Available online at www.sciencedirect.com
ScienceDirect
Journal of Colloid and Interface Science 310 (2007) 570–589
JOURNAL OF Colloid and Interface Science
www.elsevier.com/locate/jcis

Emulsification in turbulent flow: 3. Daughter drop-size distribution

Slavka Tcholakova [a], Nina Vankova [a], Nikolai D. Denkov [a,*], Thomas Danner [b]

[a] *Laboratory of Chemical Physics & Engineering, Faculty of Chemistry, Sofia University, 1 James Bourchier Ave., 1164 Sofia, Bulgaria*
[b] *BASF Aktiengesellschaft, GCT/P, L549, Ludwigshafen, Germany*

Received 20 October 2006; accepted 20 January 2007

Available online 14 February 2007

Abstract

Systematic set of experiments is performed to clarify the effects of several factors on the size distribution of the daughter drops, which are formed as a result of drop breakage during emulsification in turbulent flow. The effects of oil viscosity, η_D, interfacial tension, σ, and rate of energy dissipation in the turbulent flow, ε, are studied. As starting oil–water premixes we use emulsions containing monodisperse oil drops, which have been generated by membrane emulsification. By passing these premixes through a narrow-gap homogenizer, working in turbulent regime of emulsification, we monitor the changes in the drop-size distribution with the emulsification time. The experimental data are analyzed by using a new numerical procedure, which is based on the assumption (supported by the experimental data) that the probability for formation of daughter drops with diameter smaller than the maximum diameter of the stable drops, $d < d_{MAX}$, is proportional to the drop number concentrations in the final emulsions, which are obtained after a long emulsification time. We found that the breakage of a single "mother" drop leads to the formation of multiple daughter drops, and that the number and size distribution of these daughter drops depend strongly on the viscosity of the dispersed phase. Different scaling laws are found to describe the experimental results for the oils of low and high viscosity. The obtained results for the daughter drop-size distribution are in a reasonably good agreement with the experimental results reported by other authors. In contrast, the comparison with several basic model functions, proposed in the literature, does not show good agreement and the possible reasons are discussed. The proposed numerical procedure allows us to describe accurately the evolution of all main characteristics of the drop-size distribution during emulsification, such as the number and volume averaged diameters, and the distributive and cumulative functions by number and by volume. The procedure allowed us to clarify the relative importance of the drop breakage rate constant and of the daughter drop-size distribution for the evolution of the various mean diameters.

Keywords: Drop breakage; Emulsification in turbulent flow; Drop-size distribution; Daughter drops; Satellite drops

1. Introduction

In the previous papers of this series [1,2] we presented experimental results for the maximum diameter of the stable drops, mean drop diameter, emulsion polydispersity, and drop breakage constants for a series of oil-in-water-emulsions, obtained by emulsification in turbulent flow. The experiments were performed at high surfactant concentration to avoid drop–drop coalescence during emulsification. The effects of drop size, oil viscosity, interfacial tension, and rate of energy dissipation were quantified and discussed. The observed effects of these factors on the maximum drop diameter were described by the model of Kolmogorov–Hinze [3,4], and its upgraded version for viscous oils by Davies, Calabrese et al., and Lagisetty et al. [5–10]. The experimental results for the breakage rate constants were described quantitatively by modifications of existing theoretical models [2].

In the current paper we continue our studies of emulsification in turbulent flow [1,2,11–13] by analyzing the effects of the same factors on the probability for formation of smaller ("daughter") droplets upon breakage of a larger ("mother") drop. The same raw experimental data, which were used in Ref. [2] to determine the drop breakage rate constants, k_{BR},

* Corresponding author. Fax: +359 2 962 5643.
E-mail address: nd@lcpe.uni-sofia.bg (N.D. Denkov).

0021-9797/$ – see front matter
doi:10.1016/j.jcis.2007.01.097

are used here to determine the daughter drop-size distribution. For this reason, we do not represent in the current paper the experimental methods and materials, and the detailed kinetic scheme—these are described in Ref. [2]. Only some of the main equations are reproduced here to facilitate the reader.

Three major groups of models about the probability for daughter drop formation are proposed in the literature—statistical, phenomenological (based on the change in the surface energy of the breaking drops), and hybrid models (a combination of the previous two), see the comprehensive review by Lasheras et al. [14] and Section 5.5 below. The various models predict rather different probabilities for formation of daughter drops with given size. For example, some of the models predict maximum probability for formation of drops with equal size (i.e., with volume $\approx 1/2$ of the volume of the mother drop) [15,16], whereas other models predict that the probability for formation of such equally sized drops is minimal [17–19]. The attempts to interpret our experimental data by these models showed, however, that neither of them could be directly used to describe our systems—see Section 5.5 below. Therefore, another approach was necessary to describe the experimental data.

In several studies the size distribution of the daughter drops was investigated experimentally by optical observation of the breakage of single drops in turbulent flow [20,21]. The effects of drop size and interfacial tension were studied. The experiments in Ref. [21] were performed with heptane only as oil phase, so that the effect of oil viscosity was not studied. On the other hand, numerous studies of the breakage process in shear flow demonstrated that the increase of the dispersed phase viscosity leads to a larger number of formed drops at equivalent all other conditions [22–24]. This effect of the oil viscosity on the size distribution of the daughter drops formed in turbulent flow has not been clarified so far and deserves further investigation. Just as example, the experiments on emulsification in turbulent flow evidence that the emulsion polydispersity significantly increases with oil viscosity [1,6–9]. As we show below, this effect can be explained with the effect of oil viscosity on the total number and the size distribution of the formed daughter drops.

The paper is organized as follows: In Section 2 we describe the experimental data for the evolution of the drop-size distribution in the emulsions, as a function of the emulsification time. The kinetic scheme used for interpretation of the experimental data is explained in Section 3. The procedure for determination of the daughter drop-size distribution is given in Section 4. The results for the various systems, as well as their comparison with the experimental results by other authors and with theoretical models are described in Section 5. Section 6 summarizes the main results and conclusions.

2. Experimental results—Evolution of the drop-size distribution during emulsification

In this section we present experimental results for the evolution of the drop-size distribution in the emulsions, as a function of the emulsification time. For each system, series of histograms were constructed from the measured drop diameters after different number of passes, u, of the emulsion through the homogenizer. These histograms were processed to determine the number concentration, n_S, of the drops falling within a given size interval as a function of the number of passes, that is, as a function of the emulsification time, $t_{EM} = u\theta$, where θ is the residence time of the drops in the active zone of the homogenizer [2].

As explained in Section 3.2 of Ref. [2], the histograms were obtained by classifying the measured drop diameters into discrete intervals with average diameters $d_S = \sqrt[3]{2^S} d_0$ ($0 \leqslant S \leqslant N$), so that $d_{S+1}/d_S = 2^{1/3}$. The diameter $d_0 = 0.25$ μm corresponds to the interval of the smallest drops, whereas N is the index of the interval corresponding to the largest drops in the emulsion. The width of the intervals is proportional to the mean drop diameter for the respective interval, $\Delta y_S = 0.23 d_S$—see Eq. (1) in Ref. [2]. The number concentration of the drops falling in a given interval was determined by the mass balance:

$$n_S(d_S) = \frac{N_S}{V_{EM}} = \frac{N_S \Phi}{V_{OIL}} = \frac{6\Phi}{\pi} \frac{N_S}{\sum_{i=0}^{N} N_i d_i^3}, \tag{1}$$

where N_S is the number of measured drops falling in the interval with average diameter d_S, Φ is oil volume fraction, V_{EM} is emulsion volume, and V_{OIL} is total volume of emulsified oil.

From a series of histograms corresponding to different numbers of passes of a given emulsion through the homogenizer, we could analyze the process of drop breakage. The exact procedure used for determination of the probability, $p_{S,M}$, for formation of drops with diameter d_S after breaking a drop with diameter d_M is described in Section 4 below. Here we describe briefly only the main trends seen in the histograms. These trends are essentially used in Section 4 to define the procedure for determination of $p_{S,M}$.

A series of histograms for the hexadecane emulsion stabilized by Brij 58 (denoted as C16_Br_p1 in Table 1 of Ref. [2]), before its passage through the narrow-gap homogenizer, as well as after 1, 5, 10, 20, and 100 passes is presented in Fig. 1. One sees from Fig. 1A that the number concentration of the drops with $d > 20$ μm $\approx 2.2 d_D$ (where $d_D \approx 9$ μm is the maximum drop diameter at steady state, calculated by Eq. (15) in Ref. [2]) decreases rapidly to zero in the first 5 passes, whereas the concentration of the drops with diameters 10 μm $< d <$ 20 μm decreases more gradually, Fig. 1. These changes in the number concentration of the large drops in the emulsions are directly related to the breakage rate constant, $k_{BR}(d)$, see the discussion in Section 5 of Ref. [2]. As seen from Fig. 1, the reduction of the number concentration of the drops with $d > 10$ μm $\approx 1.1 d_D$, is accompanied with a significant increase of the number concentration of the smaller drops with $d < 10$ μm. As explained in Ref. [2], the breakage of the drops with diameter $d < d_D$ is relatively slow in the time scale of our emulsification experiments.

Let us consider in more detail the shape of the histograms in the region of the small drops, $d < d_D \approx 9$ μm, see Fig. 1. For this particular emulsion, we see that the drop number concentration is almost constant for the drops with diameters between 1 and 5 μm (after a given pass) and gradually increases with the number of passes, u (see Fig. 1B). The number concentration of the drops with diameter $d < 1$ μm also increases with u, but

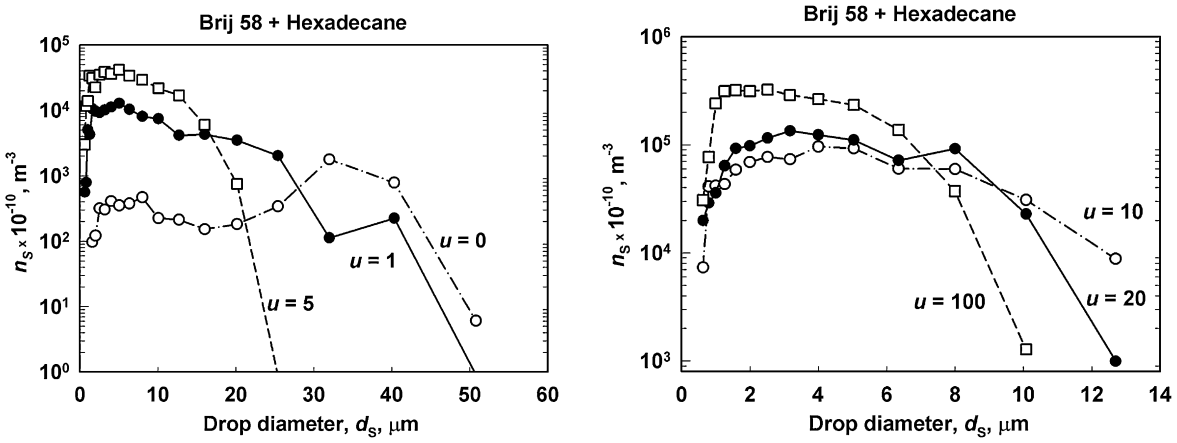

(A) (B)

Fig. 1. Number concentration of drops, $n(d_S)$, as a function of the drop diameter in emulsion of hexadecane stabilized by 1 wt% Brij 58 (denoted as C16_Br_*P*1 in Table 1 of Ref. [2]) after different number of emulsion passes, u, through the narrow-gap homogenizer: (A) $u = 0$ (in the initial premix), and after 1 and 5 passes; (B) after 10, 20, and 100 passes.

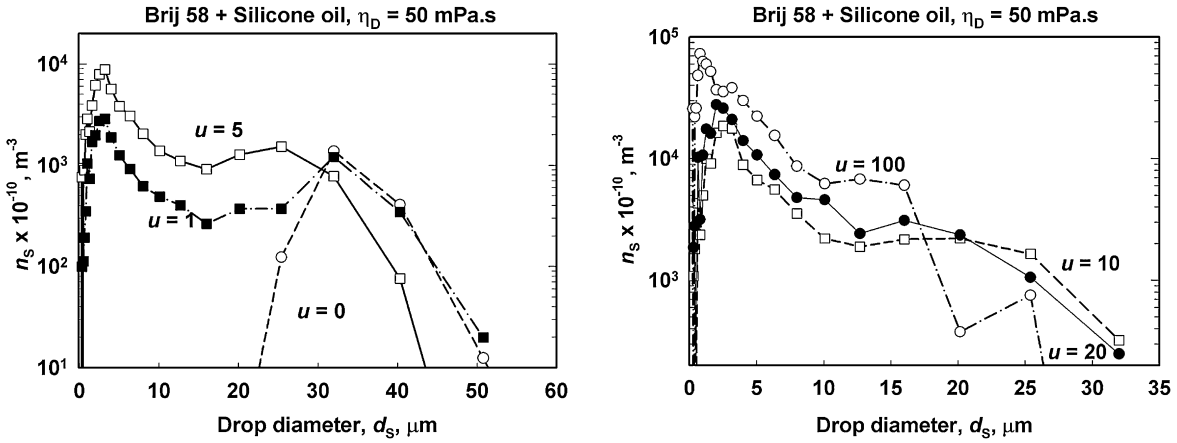

(A) (B)

Fig. 2. Number concentration of drops, $n(d_S)$, as a function of the drop diameter in emulsion of silicone oil 50 stabilized by 1 wt% Brij 58 (denoted as Sil50_Br_*P*1 in Table 1 of Ref. [2]) after different number of emulsion passes, u, through the narrow-gap homogenizer: (A) $u = 0$ (in the initial premix), and after 1 and 5 passes; (B) after 10, 20, and 100 passes.

their concentration after a given pass is significantly lower than the concentration of the drops with diameters between 1 and 5 μm. From these results we can conclude that the drops with diameter between 1 and 5 μm are formed with similar probability, which is much higher than the probability for formation of drops with $d < 1$ μm. Similar trends were observed for hexadecane emulsions stabilized by Na caseinate (data not shown in Fig. 1).

For the emulsions prepared with more viscous silicone and soybean oils, well-pronounced peaks were observed in the histograms at $d < d_D$. For example, in the emulsion of silicone oil with viscosity $\eta_D = 50$ mPa s, the drops with diameter around 2.5 μm have maximum number concentration after each pass, u, see Fig. 2 (the drops with diameter below 1 μm, which are observed in some of these systems after 100 passes, will not be discussed in the paper, because their size is comparable to the optical resolution of the microscope). Taking into account the fact that all drops with diameter $d < d_D \approx 20$ μm are obtained as a result of breakage of drops with diameter $d > d_D$, we can deduce that the peak observed at $d \approx 2.5$ μm should reflect a maximum in the probability for formation of these droplets upon breakage of the large drops in the emulsion. Therefore, the observed qualitative difference in the histograms of the hexadecane emulsions on one side, and the emulsions of more viscous oils on the other side, indicates that the probability for formation of daughter drops is qualitatively different in these two systems: the drops with diameter between 1 and 5 μm are formed with similar probability in the hexadecane emulsions, whereas daughter drops with preferred size (corresponding to the peaks in the histograms) are observed with the more viscous oils.

Interestingly, we observed two well-defined peaks in the histograms for the viscous silicone oil with $\eta_D \approx 500$ mPa s after the first several passes: one peak around 4 μm and another peak around 2 μm, see Fig. 3. The ratio of the heights of these two peaks is ≈2:1. Taking into account the fact that the width of the size intervals around 4 μm is about 2 times larger than the interval width around 2 μm, one can deduce that for every drop with diameter 4 μm, approximately one drop with diameter 2 μm

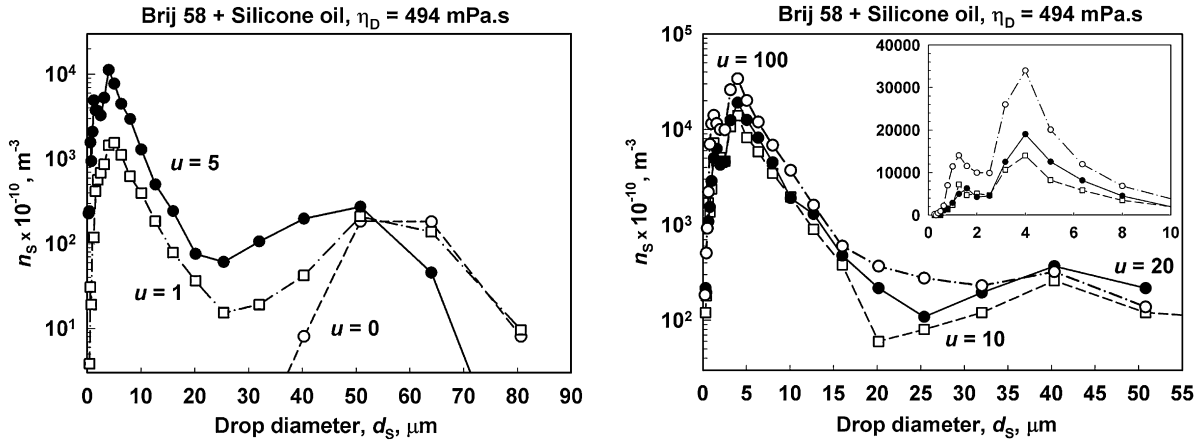

(A) (B)

Fig. 3. Number concentration of drops, $n(d_S)$, as a function of the drop diameter in emulsion of silicone oil 500 stabilized by 1 wt% Brij 58 (denoted as Sil500_Br_*P*2) after different number of emulsion passes, u, through the narrow-gap homogenizer: (A) $u = 0$ (in the initial premix), and after 1 and 5 passes; (B) after 10, 20, and 100 passes. The inset in (B) shows expanded the region of small drops after 10, 20, and 100 passes.

is formed during emulsification. We could speculate that these two peaks are due to the formation of the so-called "satellite" and "sub-satellite drops," well known in the studies of drop breakage in shear flows [22–24]. Interestingly, similar in shape bimodal drop-size distributions were predicted theoretically by Kostoglou and Karabelas [25] by solving the population balance equation with certain model assumptions for the daughter drop-size probability, based on the statistical characteristics of the turbulent flow and of the drop-eddy collision frequency.

In conclusion, the number concentration of the drops is low for drops with diameter smaller than 1 μm in all systems studied. Depending on the oil viscosity, the number concentration of the drops with diameters between 1 and 5 μm could be similar (hexadecane), passes through one maximum (silicone oil and soybean oil with viscosity 50 mPa s), or passes through two maximums (silicone oils with viscosity 200 and 500 mPa s). Note that the shapes of the histograms shown in Figs. 1–3 are affected by the variable widths of the intervals. Therefore, it is more instructive to discuss in detail the probability for drop formation after normalizing the experimental points in the histograms by the interval widths—see Section 5 below.

3. Kinetic scheme for data interpretation

From the drop-size histograms we could determine the dependence of the number concentration of drops with given diameter on the number of emulsion passes through the homogenizer, u. From these dependences we can determine the breakage rate constants and the probability for formation of daughter drops, $p_{S,M}$. The main assumptions used to formulate the kinetic scheme for data interpretation are explained in Section 3 of Ref. [2]. Here we present only the basic equations.

As explained in Ref. [2], from the drop-size histograms and their interpretation, we can define three types of drops in the emulsions studied: (i) largest drops with diameter d_N, which can only break, (ii) drops with diameter between d_K and d_N, which can simultaneously break and form from breaking larger drops, and (iii) drops with diameter equal or smaller than d_K, which cannot break and are only formed from drops with diameter larger than d_K. The kinetic equation describing the evolution of the concentration of the largest drops in the emulsion, $n_N(x)$, is

$$U_1 \frac{\mathrm{d}n_N(x)}{\mathrm{d}x} = -k_N n_N(x), \tag{2}$$

where U_1 is the average linear velocity of the fluid along the processing element, x is the distance from the beginning of the processing element (considered as a reactor of ideal displacement), and k_N is the breakage rate constant for the largest drops.

The equation describing the number concentration, n_S, of drops with diameter d_S, which could simultaneously break and form from larger drops, is

$$U_1 \frac{\mathrm{d}n_S(x)}{\mathrm{d}x} = -k_S n_S(x) + \sum_{M=S+1}^{N} 2^{M-S} p_{S,M} k_M n_M(x) \quad \text{for } K < S < N, \tag{3}$$

where the first term in the right-hand side gives the rate of drop breakage, whereas the second term describes the rate of formation of these drops.

For the drops with diameter smaller or equal to d_K the first term in Eq. (3) is zero:

$$U_1 \frac{\mathrm{d}n_S(x)}{\mathrm{d}x} = \sum_{M=K+1}^{N} 2^{M-S} p_{S,M} k_M n_M(x) \quad \text{for } 0 \leqslant S \leqslant K. \tag{4}$$

In the above equations, $p_{S,M}$ denotes the average fraction of the volume of the "mother" drop with diameter d_M, which is transformed into drops with diameter d_S, where $0 \leqslant S \leqslant (M-1)$. Correspondingly, the product $(2^{M-S} p_{S,M})$ gives the average number of drops with diameter d_S, which are formed as a result of breakage of one drop with diameter d_M. The mass balance of the volume of breaking drop requires [2]:

$$\sum_{S=0}^{M-1} p_{S,M} = 1 \quad \text{for every } K < M \leqslant N. \tag{5}$$

The set of Eqs. (2)–(4) is solved for all passes of the emulsion through the homogenizer, by using as initial condition:

$$n_S(u=0) = n_S^0 \quad \text{for } 0 \leqslant S \leqslant N, \tag{6}$$

where n_S^0 is the number concentration of the drops with diameter d_S in the initial premix (before emulsion passage through the homogenizer).

To determine the breakage rate constants $k_S(d_S)$ and the probabilities $p_{S,M}(d_S, d_M)$, we compare the experimentally determined number concentrations of the drops at the outlet of the homogenizer (after different numbers of passes, u) with the solution of the above set of equations. For this comparison we calculate the number concentrations of the drops at the end of the reactor ($x = L$) after each pass through the homogenizer, and consider k_S and $p_{S,M}$ as adjustable parameters, which have to be determined from the comparison of the theoretical predictions for $n_S(u)$ with the experiment data for all drops in the emulsion.

The constructed kinetic scheme (see also Section 3 in Ref. [2]) contains a set of $(N+1)$ equations for the number concentrations of drops with diameters $\{d_0, \ldots, d_N\}$, plus $(N-K)$ equations expressing the mass balance of the breaking drops with size $\{d_{K+1}, \ldots, d_N\}$, see Eq. (5). On the other hand, we have $(N-K)$ unknown breakage rate constants for the drops with $d_S > d_K$, as well as $(N-K)(N+K+1)/2$ unknown constants of type $p_{S,M}$. Since the total number of unknown constants is larger than the total number of equations, we should make some additional assumptions for $p_{S,M}$ to solve the set of equations. Several models for $p_{S,M}$ were tested, as described in the following Section 4.

4. Determination of the probabilities $p_{S,M}$ from the experimental data

In this section we describe the numerical procedure used for determination of $p_{S,M}$ from the experimental data. We tested several models for the daughter drop-size distributions, starting from the simplest possible model of binary breakage with formation of two equally sized drops.

4.1. Binary breakage into equally sized drops

In our terms, the simplest model of "binary breakage" [14,15,26] implies that only drops with equal diameters, d_{M-1}, are formed after breakage of a drop with diameter $d_M (K < M \leqslant N)$. Therefore, this model requires $p_{M-1,M} = 1$ and $p_{S,M} = 0$ for all values of $S < M-1$. Note that according to this model, formation of drops with diameter smaller than d_K is impossible, because the smallest drops that can break are those with diameter d_{K+1}. This limitation of the binary breakage model is in obvious contradiction with the experimental data, because a significant fraction of drops with $d < d_K$ are seen in the final emulsions, even when the initial premix did not contain any such drops, see Figs. 1–3. Therefore, this model is unable to describe any of the systems studied.

4.2. Equal number probability for drop formation

Another hypothetical case, which leads to relatively simple closed set of equations, can be designed by assuming that the breakage of a drop with diameter d_M results in the formation of a series of single drops with diameters $\{d_{M-1}, d_{M-2}, \ldots, d_1\}$, all of them with equal probability [27], plus two smallest drops with diameter d_0:

$$p_{S,M} = 1/2^{(M-S)} \quad \text{for } 1 \leqslant S \leqslant M-1 \text{ and } p_{0,M} = 1/2^{(M-1)}. \tag{7}$$

Two droplets with diameter d_0 are assumed to form in this model in order to satisfy precisely the mass balance, Eq. (5). Since these smallest droplets have negligible contribution into the total mass balance of the formed daughter drops, this assumption has no significant effect on the final results of the calculations and on the conclusions.

In the framework of this model, we should determine only the breakage rate constants from the experimental data, because the values of $p_{S,M}$ are defined by Eq. (7). Note that this model allows the formation of drops with $d < d_K$, in agreement with the experimental results.

Direct comparison of the predictions of this model with our experimental data showed that the estimated probability for drop formation is strongly over-predicted for all drops with diameter d smaller than ca. $0.1d_D \approx 1$–2 μm for the hexadecane emulsions. In contrast, for all emulsions of the more viscous oils, this model under-predicts the formation of drops with $d < 0.3d_D \approx 5$–10 μm. These comparisons evidence that the probability $p_{S,M}$ is not the same for emulsions of oils with low and high viscosity (as assumed in this model), and that a more complex model, accounting for the effect of oil viscosity, is needed to describe all systems studied.

We found that the equal-probability model, Eq. (7), could be slightly modified to describe reasonably well the data for the hexadecane emulsion stabilized by Brij 58. Direct numerical check showed that for this system, the equal number probability for drop formation could be applied for all drops with $d > 1$ μm, see Fig. 4. For all other emulsions, the "equal probability" model predicts results, which are rather different from the experimental data.

4.3. Non-equal number probability for drop formation (combined model)

The comparison of the experimental data with the predictions of the "equal number probability" model (Section 4.2), showed that this model described reasonably well the evolution of the drops with $d > d_K$ in most of the emulsions, where d_K is the diameter of the largest drops that could not break [2].

On the other hand, it is seen from Figs. 1–3 that the shape of the histograms for all drops with $d < d_K$ is well preserved after the first several passes of the emulsion through the homogenizer, despite the fact that the size of the breaking largest drops in the emulsions significantly decreases with the number of passes. The latter observation leads to the very important

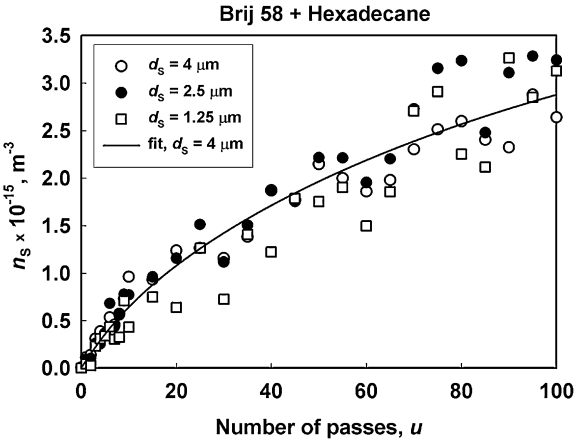

Fig. 4. Number concentrations of drops, $n(d_S)$, as a function of the number of emulsion passes through the homogenizer for hexadecane emulsion stabilized by Brij 58 (C16_Br_$P1$) for the daughter drops with diameter in the range 1 μm $< d < d_K = 5$ μm. The points are experimental data, whereas the curve is a fit, according to the model of equal number probability (Section 4.2).

conclusion that the probability for formation of the drops with $d < d_K$ does not depend significantly on the diameter of the breaking mother drops, i.e., the self-similarity assumption is not valid for the daughter drops with size $d < d_K$. These two observations suggested us to try a combination of two qualitatively different sets of probabilities for the two regions of drop diameters (above and below d_K) in an attempt to design a function, $p_{S,M}$, which is able to describe both regions simultaneously.

With this aim in view, we first tested the following procedure:

(1) The number probability, $2^{M-S}p_{S,M}$, was assumed to be equal for all drops with $d > d_K$:

$$2^{M-S}p_{S,M} = b_1 \quad \text{for } K < S \leqslant M-1, \tag{8}$$

where the value of the adjustable constant b_1 was determined (along with the values of the kinetic constants k_S) from the best fit to the experimental data.

(2) In agreement with the experimental data (Figs. 1–3), the probability for formation of drops with $d \leqslant d_K$ was assumed to be proportional to the number concentration of the respective drops in the final emulsion (after 100 passes through the homogenizer):

$$2^{M-S}p_{S,M} = b_M n_S(u=100) \quad \text{for } 0 \leqslant S \leqslant K, \tag{9}$$

where, for a given emulsion, the proportionality constant $b_M(d_M)$ does not depend on the size of the daughter drop, d_S, and is determined from the mass balance (see Eq. (5)):

$$b_M = \left[1 - b_1\left(1 - 2^{K-M+1}\right)\right] \Big/ \sum_{i=0}^{K}\left(n_i(u=100)/2^{M-i}\right). \tag{10}$$

Assumption 2 (expressed through Eq. (9)) was made with the idea that the final drop-size distribution, obtained after 100 passes of the emulsion through the homogenizer, reflects the probabilities for formation of the daughter drops in the preceding passes. Indeed, with the set of Eqs. (8)–(10) for $p_{S,M}$ we were able to describe the evolution of the drop number concentrations with rather good accuracy for most of the emulsions studied. In particular, the model described very well the drops with $d < d_K$ for all emulsions. However, we observed systematic deviations of the theoretical curves $n_S(u)$ from the respective experimental data for the large drops with $d > d_K$, for which maximums in the curves $n_S(u)$ were experimentally observed (like the curve shown in Fig. 5B of Ref. [2]). The performed analysis showed that these deviations were related to the assumed equal number probability for formation of these large drops (Eq. (8)).

Therefore, we upgraded the above model by assuming that the ratio of the probabilities for formation of the two largest daughter drops with diameters d_{M-1} and d_{M-2} does not depend on the diameter of the mother drop, d_M:

$$p_{M-1,M}/p_{M-2,M} = b_2 = \text{const} \quad \text{for arbitrary } M. \tag{11}$$

The number probability for formation of drops in the intervals from K to $(M-2)$ was again assumed to be equal and was calculated by a counterpart of Eq. (8):

$$2^{M-S}p_{S,M} = b_3 \quad \text{for } K < S \leqslant M-2, \tag{12}$$

where the constant b_3 was found by matching the probabilities calculated from Eqs. (9) and (12) for the drops with size d_K:

$$b_3 = b_M n_K(u=100). \tag{13}$$

For the probability for formation of drops with diameter $d < d_K$, we used Eq. (9) and the value of the constant b_M was found from the corresponding mass balance:

$$b_M = \left[\left(1 - 2^{K-M+1} + b_2/2\right)n_K/2 + \sum_{i=0}^{K-1} n_i/2^{M-i}\right]^{-1}. \tag{14}$$

Let us summarize here the main assumptions of this final model for $p_{S,M}$, which was found to describe the experimental data for all emulsions studied: We split the size distribution of the formed daughter drops into two regions—small daughter drops with diameter $d_S \leqslant d_K$ and large daughter drops with diameter $d_S > d_K$. The number probability for formation of the small daughter drops ($d_S \leqslant d_K$) is assumed proportional to the number concentration of the respective drops in the final emulsion, Eq. (9). The constant of proportionality, b_M, depends on the size of the breaking mother drop, d_M, and is determined from the mass balance, Eq. (14). The number probability for formation of the large drops ($d_K < d_S < d_{M-1}$) is assumed equal to the respective probability for the drops with size d_K (Eqs. (12) and (13)). For the largest daughter drops ($d_S = d_{M-1}$), the number probability is assumed proportional to that of d_K with a constant of proportionality, denoted by b_2 (Eq. (11)), which does not depend on d_M and u.

Therefore, in this version of the model we have only one adjustable parameter, b_2, which was determined (along with the values of the kinetic constants k_S) from the best fit to the experimental data, $n_S(u)$, for all drops and for all passes of the emulsion through the homogenizer. We found that this model described rather well the experimental data for all emulsions studied. The results presented and discussed below, as well as

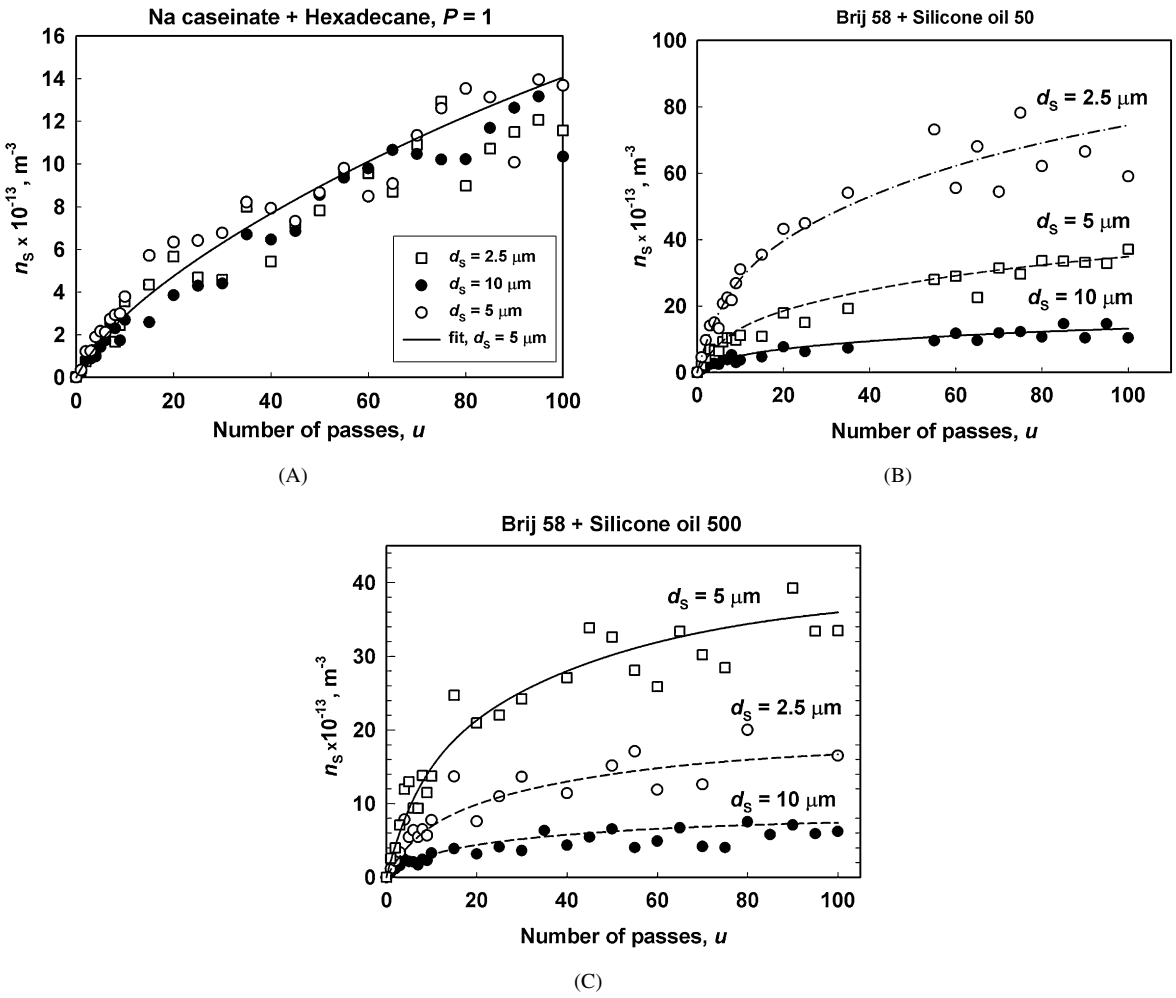

Fig. 5. Number concentration of drops, $n(d_S)$, as a function of the number of emulsion passes through the homogenizer for drops with different diameters: (A) hexadecane emulsion stabilized by Na caseinate (C16_NaC_*P*1); (B) emulsion of silicone oil 50 (Sil50_Br_*P*1); and (C) emulsion of silicone oil 500 (Sil500_Br_*P*1). The points are experimental data, whereas the curves are fits according to the "combined model" from Section 4.3.

all results for k_{BR} presented in Ref. [2], are obtained with the values of $p_{S,M}$, as determined from Eqs. (9), (11)–(14).

Note that the used model implies two qualitatively different size ranges for the formed daughter drops: of the small daughter drops, $d \leqslant d_K$ (Eq. (9)), which do not obey the self-similarity assumption, and of the large daughter drops, $d > d_K$ (Eqs. (12) and (13)), which exhibit self-similarity. Clearly, the model does not imply self-similarity for the entire size range of the daughter drops (which is in agreement with the experimental results), because the specific values of $p_{S,M}$ depend on the diameter of the mother drop, d_M (see also Section 5.2 below). To denote the fact that we split the drop-size distribution into two qualitatively different regions (below and above d_K), we call the proposed model "the combined model."

4.4. Illustrative results for the dependence $n_S(u)$, as described by the model from Section 4.3

For illustration of the results obtained with this model, we compare in Fig. 5 the experimental dependencies $n_S(u)$ for the daughter drops with diameters 2.5, 5 and 10 μm for hexadecane and two silicone oils, with the numerically calculated curves by the combined model from Section 4.3. One sees that the calculated curves are in very good agreement with the experimental data for all emulsions and drop sizes. For the hexadecane emulsion, the almost equal probability for drop formation of drops with diameter between 2.5 and 10 μm, after breaking of the mother drops, leads to almost equal values of n_S in all passes, see Fig. 5A. On the other hand, for the emulsion of silicone oil with viscosity 50 mPa s, the probability for formation of drops with $d \approx 2.5$ μm is around two times higher than that for drops with $d \approx 5$ μm and around seven times higher than that for drops with $d_S \approx 10$ μm—in agreement, similar ratios between the respective number concentrations $n_S(d_S)$ are observed in all passes. For the silicone oil with viscosity 500 mPa s, the number concentration of the drops with $d_S \approx 5$ μm is higher than the number concentration of the drops with $d_S \approx 2.5$ μm and 10 μm, which reflects the different probabilities for formation of the drops with these diameters, see Fig. 5C.

We can conclude that Eqs. (9), (11)–(14) and the respective procedure for determination of $p_{S,M}$ describe rather well the experimentally determined curves for $n_S(u)$ in all emulsions studied. To further verify the model, in the following subsection

we compare the experimental data for the mean drop diameters and for the drop-size distribution functions with the respective results from the numerical calculations.

4.5. Model description of the evolution of the mean drop diameters and of the drop-size distribution functions in the course of emulsification

By using the values of k_{BR} and $p_{S,M}$, determined as described in Ref. [2] and Section 4.3, we can predict the evolution of various emulsion properties (such as maximum and mean drop diameters, emulsion polydispersity, etc.), as functions of the emulsification time. Along with the changes in the drop-size histograms and in the number concentration of the drops (Figs. 1–3 and 5), other emulsion characteristics of great interest are the various mean diameters and the drop-size distribution functions. In the current section we present theoretically calculated curves for the evolution of several of these characteristics in the course of the emulsification process, and compare these curves with the respective experimental results.

The mean volume-surface diameter, d_{32}, is determined from the experimental data by the equation:

$$d_{32} = \left(\sum_i N_i d_i^3\right) \Big/ \left(\sum_i N_i d_i^2\right), \tag{15}$$

where N_i is the measured number of drops with diameter d_i. For our discrete drop-size distribution, $d_S = 2^{S/3} d_0$, the above definition is transformed to read:

$$d_{32} = d_0 \left(\sum_{S=0}^{N} 2^S n_S\right) \Big/ \left(\sum_{S=0}^{N} 2^{2S/3} n_S\right), \tag{16}$$

where n_S is the number concentration of drops in the interval centered around d_S. Equation (16) is used below to calculate the theoretical curves $d_{32}(u)$ from the numerically calculated dependences, $n_S(u)$, whereas the respective experimental data are determined by Eq. (15). In a similar way, one can determine the theoretical and experimental values of the mass-averaged mean diameter, $d_{43}(u)$.

The theoretical curves $d_{32}(u)$ and $d_{43}(u)$ were found to describe very well the experimental data for all systems studied—see for examples Figs. 6 and 7. Furthermore, the theoretical

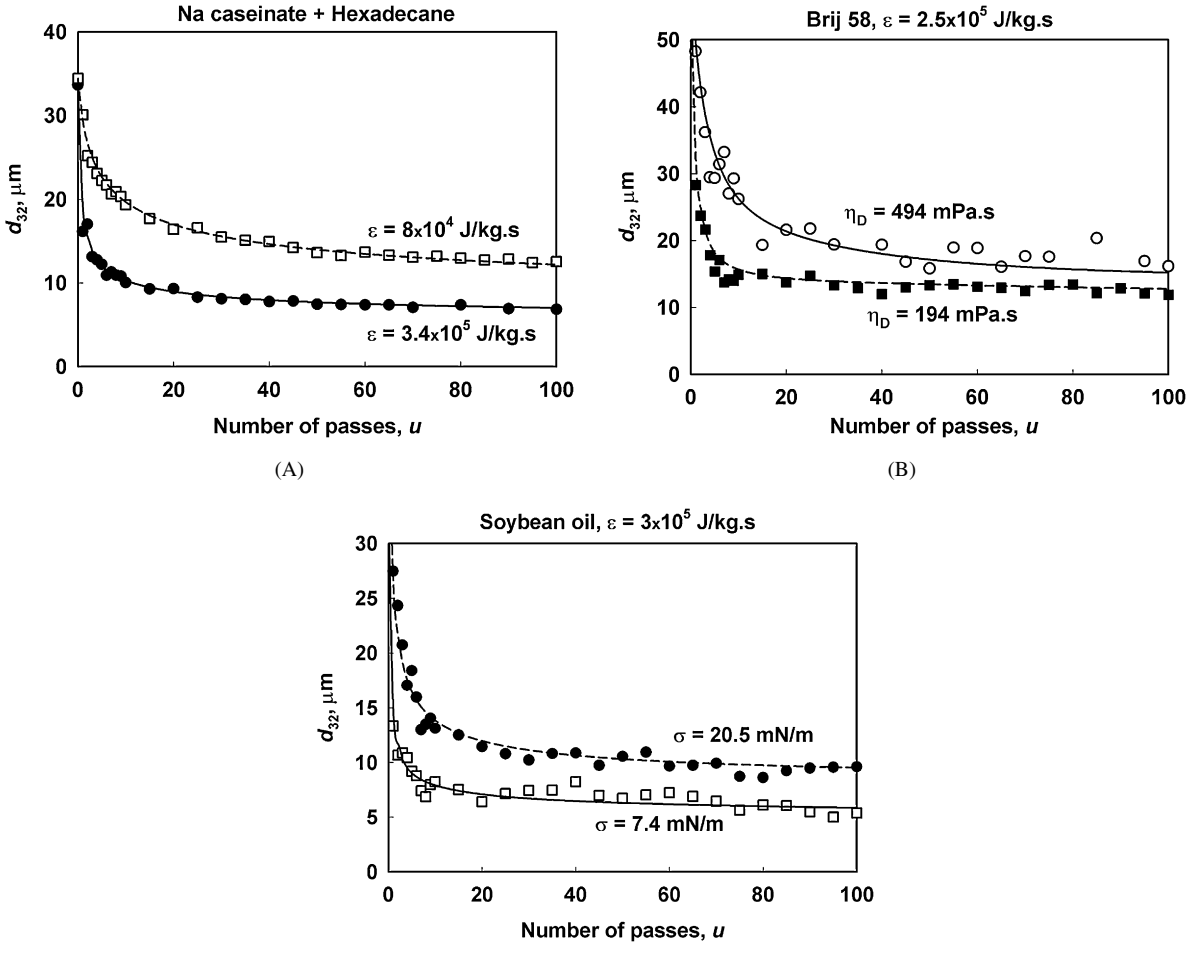

Fig. 6. Mean volume-surface diameter, d_{32}, as a function of the number of emulsion passes through the homogenizer, u: (A) hexadecane emulsions stabilized by Na caseinate, prepared at two different values of ε (C16_NaC_*P*1 and C16_NaC_*P*2); (B) silicone oils with different viscosities (Sil200_Br_*P*2 and Sil500_Br_*P*2); (C) soybean oil emulsions stabilized by Brij 58 or Na caseinate (SBO_Br_*P*2 and SBO_NaC_*P*2). The points are experimental data, whereas the curves are calculated by the model from Section 4.3.

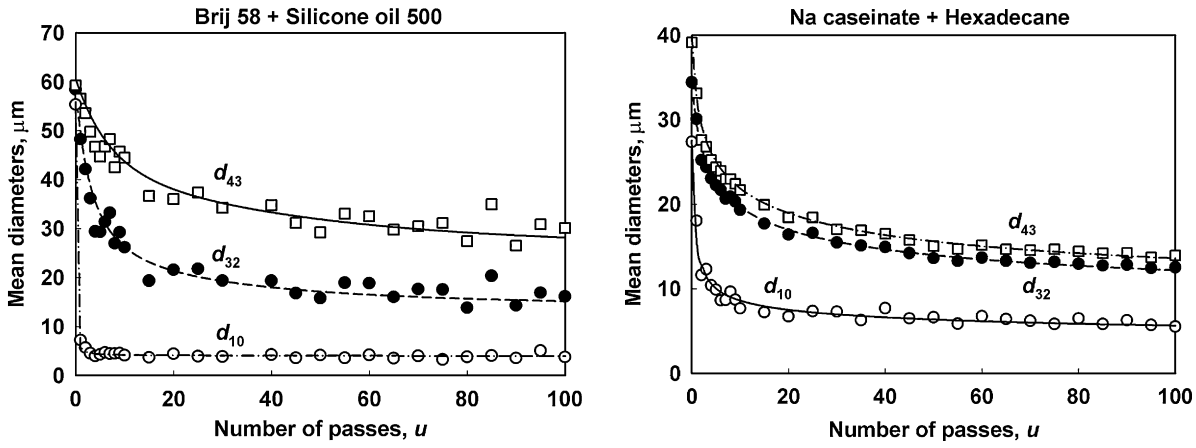

(A) (B)

Fig. 7. Mean drop diameters d_{43}, d_{32}, and d_{10}, as functions of the number of passes, u: (A) silicone oil 500 (Sil500_Br_*P*2) and (B) hexadecane (C16_NaC_*P*1). The points are experimental data, whereas the curves are calculated by the model from Section 4.3.

analysis showed that the different shapes of the curves for $d_{32}(u)$ (or $d_{43}(u)$), observed with the various emulsions, were determined mainly by the different values of k_{BR} for the largest drops in the respective systems: For the emulsions, in which the initial mean drop diameter $d_{32}(u=0)$ was much larger than d_D, both d_{32} and d_{43} decreased steeply during the first several passes of the emulsion through the homogenizer, due to the high values of k_{BR} for the large drops in the emulsion, viz. $k_{\mathrm{BR}}\theta \gg 1$, where θ is the residence time (see Table 1 in Ref. [2], and Figs. S1 and S2 in Supporting material of Ref. [2]). In contrast, for the systems in which $d_{32}(u=0)$ was close to d_D, the rate of drop-size reduction was much slower, because $k_{\mathrm{BR}}\theta \leqslant 1$, see Fig. 7A. Therefore, the shape of the curves $d_{32}(u)$ and $d_{43}(u)$ depends mainly on the value of the dimensionless product $k_{\mathrm{BR}}\theta$.

In contrast, the evolution of the mean number diameter, d_{10}, defined as

$$d_{10} = \left(\sum_i N_i d_i\right) \Big/ \left(\sum_i N_i\right) = d_0 \left(\sum_{S=0}^{N} 2^{S/3} n_S\right) \Big/ \left(\sum_{S=0}^{N} n_S\right), \tag{17}$$

was found to depend mainly on the size distribution of the formed daughter drops, that is, on the values of $p_{S,M}$. Furthermore, we found that the size distribution of the daughter drops was decisive for the polydispersity of the formed emulsions. To illustrate these relations, we compare in Fig. 7 the evolution of several mean drop diameters (d_{43}, d_{32} and d_{10}), whose ratio could be used as a measure of emulsion polydispersity [28].

In Fig. 7A, we plot the functions $d_{10}(u)$, $d_{43}(u)$, and $d_{32}(u)$ for emulsion of silicone oil with $\eta_D \approx 500$ mPa s. For this viscous oil, more than 300 smaller drops are formed upon breakage of one large drop, see Table 1 in Ref. [2]. As a result, the mean number diameter d_{10} decreases from 55 down to 6 μm after the first pass of the emulsion through the homogenizer, Fig. 7A. Further, much slower decrease from 6 to 4 μm is observed during the subsequent 99 passes. On the other hand, the value of d_{43} decreases only slightly, from 60 to 58 μm after the first pass, followed by a two-fold decrease during the next 99 passes (from 58 to 28 μm). This very different kinetics of the changes in d_{10} and d_{43} for silicone oil emulsions is due to the very different probabilities for formation of daughter drops with diameters above and below d_D, see Section 5.1 below for further discussion on this point.

The results for hexadecane emulsion (oil viscosity $\eta_D =$ 3 mPa s) are shown in Fig. 7B. The comparison of Figs. 7A and 7B evidences that d_{43} for hexadecane decreases faster, whereas d_{10} decreases much more slowly, as compared to the emulsion of the viscous silicone oil. This comparison shows also that the hexadecane emulsions are significantly less polydisperse than the emulsions of silicone oil, during the entire emulsification process. For example, in the final emulsions $d_{43}/d_{32} \approx 1.1$ and $d_{43}/d_{10} \approx 2.5$ for hexadecane, whereas $d_{43}/d_{32} \approx 2$ and $d_{43}/d_{10} \approx 8$ for the silicone oil, cf. Figs. 7A and 7B.

We can conclude from these comparisons that the various mean drop diameters could evolve rather differently. The evolution of the number mean diameter, d_{10}, and the polydispersity of the formed emulsion are determined mainly by the daughter drop-size distribution (which in turn depends strongly on oil viscosity), whereas the evolution of the mass-averaged and the maximum diameters (d_{43}, d_{32}, d_{V95}) is determined mainly by the rate constants k_{BR} for the largest drops in the system.

At the end of this section, we compare the experimental results with the numerically calculated cumulative functions by volume, $F_V(d)$, for hexadecane and silicone oil emulsions after different number of passes of these emulsion through the homogenizer, $u = 0$, 5, 20, and 100. As one can see from Fig. S1 in Supplementary material to this paper, the agreement between the experimental data and the calculated curves is satisfactory, which is an additional confirmation that the proposed numerical procedure, Eqs. (9) and (11)–(14), describes rather well the entire set of main characteristics of the emulsions studied.

5. Results and discussion of the size distribution of the daughter drops

In Section 5.1 we define the functions, which are used in the current section for comparison of the daughter drop-size distributions. In Sections 5.2 and 5.3 we compare the size distributions of the daughter drops formed in the various emulsions, as determined in our experiments. In Sections 5.4 and 5.5, our results are compared with experimental results and model distributions from the literature.

5.1. Definitions of the various size distribution functions of the daughter drops

As explained in Section 3, $p_{S,M}$ is defined as the volume fraction of the breaking drop with diameter d_M (corresponding to volume $v_M = 2^M v_0$), which transforms into daughter drops falling in the interval around d_S (volume $v_S = 2^S v_0$). Therefore, the values of $p_{S,M}$ can be considered as discrete probability by volume, whereas the corresponding values of $(2^{M-S} p_{S,M})$—as discrete probability by number. Note, however, that these probabilities are defined for variable width of the intervals around d_S. To determine the respective discrete distribution functions, $\beta_V(S, M)$ and $\beta_N(S, M)$, which do not depend on the interval widths and could be directly compared with the continuous distribution functions, $\beta_V(d, d_M)$ and $\beta_N(d, d_M)$, which are usually discussed in the theoretical models [14–20, 29], one should normalize the probabilities expressed through $p_{S,M}$ by the widths of the respective intervals, $\Delta y_S = 0.23 d_S$ (see Eq. (1) in Ref. [2]):

$$\beta_V(S, M) = (p_{S,M}/\Delta y_S) \Big/ \sum_{S=0}^{M-1} p_{S,M},$$

$$\beta_N(S, M) = \left[2^{(M-S)} p_{S,M}/\Delta y_S\right] \Big/ \sum_{S=0}^{M-1} 2^{(M-S)} p_{S,M},$$

$$\Delta y_S = 0.23 d_S. \tag{18}$$

The values of $\beta_V(S, M)$ and $\beta_N(S, M)$ are discrete approximations to the continuous functions $\beta_V(d, d_M)$ and $\beta_N(d, d_M)$, which by definition give the probability (by volume and by number, respectively) for formation of daughter drops within the interval between d and δd from a mother drop with diameter d_M.

The corresponding discrete cumulative functions are defined as

$$G_V(S, M) = \sum_0^S \beta_V(S, M)\Delta y_S = \left(\sum_{j=0}^{S} p_{j,M}\right) \Big/ \left(\sum_{j=0}^{M-1} p_{j,M}\right),$$

$$G_N(S, M) = \sum_0^S \beta_N(S, M)\Delta y_S = \left(\sum_{j=0}^{S} 2^{M-j} p_{j,M}\right) \Big/ \left(\sum_{j=0}^{M-1} 2^{M-j} p_{j,M}\right). \tag{19}$$

The function $G_V(S, M)$ gives the volume fraction that is converted to daughter drops with diameter $d \leqslant d_S$, after breaking a drop with diameter d_M. Respectively, $G_N(S, M)$ gives the number fraction of the formed daughter drops with diameter $d \leqslant d_S$ (normalized with the total number of daughter drops). In the following Sections 5.2 and 5.3, we compare the experimental results for the various systems studied through the discrete functions, $p_{S,M}$, $\beta_{N,V}(S, M)$, and $G_{N,V}(S, M)$. In Section 5.4, the results for $\beta_{N,V}(S, M)$ and $G_{N,V}(S, M)$ are compared with literature data, which are represented through the corresponding continuous functions, $\beta_{N,V}(d, d_M)$ and $G_{N,V}(d, d_M)$, where the diameter of the daughter drops, d, is considered as a continuous variable.

5.2. Dependence of the size distribution of the daughter drops on the size of the breaking drop

As explained in Section 4.3, our experimental data do not follow the assumption for complete self-similarity of the size distribution of the daughter drops. In other words, the probability functions defined in Section 5.1 do not scale with (d_S/d_M) and depend on the size of the breaking "mother" drop, d_M.

To illustrate this dependence, we plot in Figs. 8 and 9 the results for the various probability functions for a hexadecane emulsion (case C16_NaC_p2 in Table 1 in Ref. [2]), at four different diameters of the mother drop, $d_M = 10$, 20, 40, and 80 μm. As one could deduce from the procedure used to determine $p_{S,M}$ from the experimental data (Section 4.3), when the results for the various functions are plotted versus the daughter drop diameter, d_S, the data for $d_S < d_{K+1}$ remain almost constant, whereas the points for the larger drops, $d_S \geqslant d_{K+1}$, shift to the left to account for the decreasing diameter of the breaking drop (see Fig. 8A). The height of the experimental points for given diameter d_S slightly increases with the decrease of d_M (to satisfy the mass balance), but this effect is relatively small. Alternatively, if the results are plotted versus the scaled diameter, d_S/d_M, all points shift to the right to account for the decrease of the scaling factor, d_M (e.g., Figs. 8B–8D). Therefore, in the general case, one should consider the dependence of the probability functions on d_M. In the following discussion, we present results for both ranges of breaking drop diameters, those corresponding to $d_M > d_{K+1}$ (large breaking drops, Figs. 10–11) and those corresponding to $d_M = d_{K+1}$ (smallest breaking drops, Figs. 12–13). The discussion is focused, however, mostly on those features of the functions, which do not depend significantly on d_M.

The most important feature of the results for hexadecane shown in Figs. 8–9, is the existence of a relatively wide range of diameters of daughter drops, $0.1 d_{K+1} < d_S < d_{K+1}$ (spanning three decades of daughter drop volumes), for which the distribution functions satisfy well the following scaling laws (see the straight portions of the curves describing the experimental data in Figs. 8–9):

$$d_M \beta_N(S, M) \propto (d_S/d_M)^{-1},$$

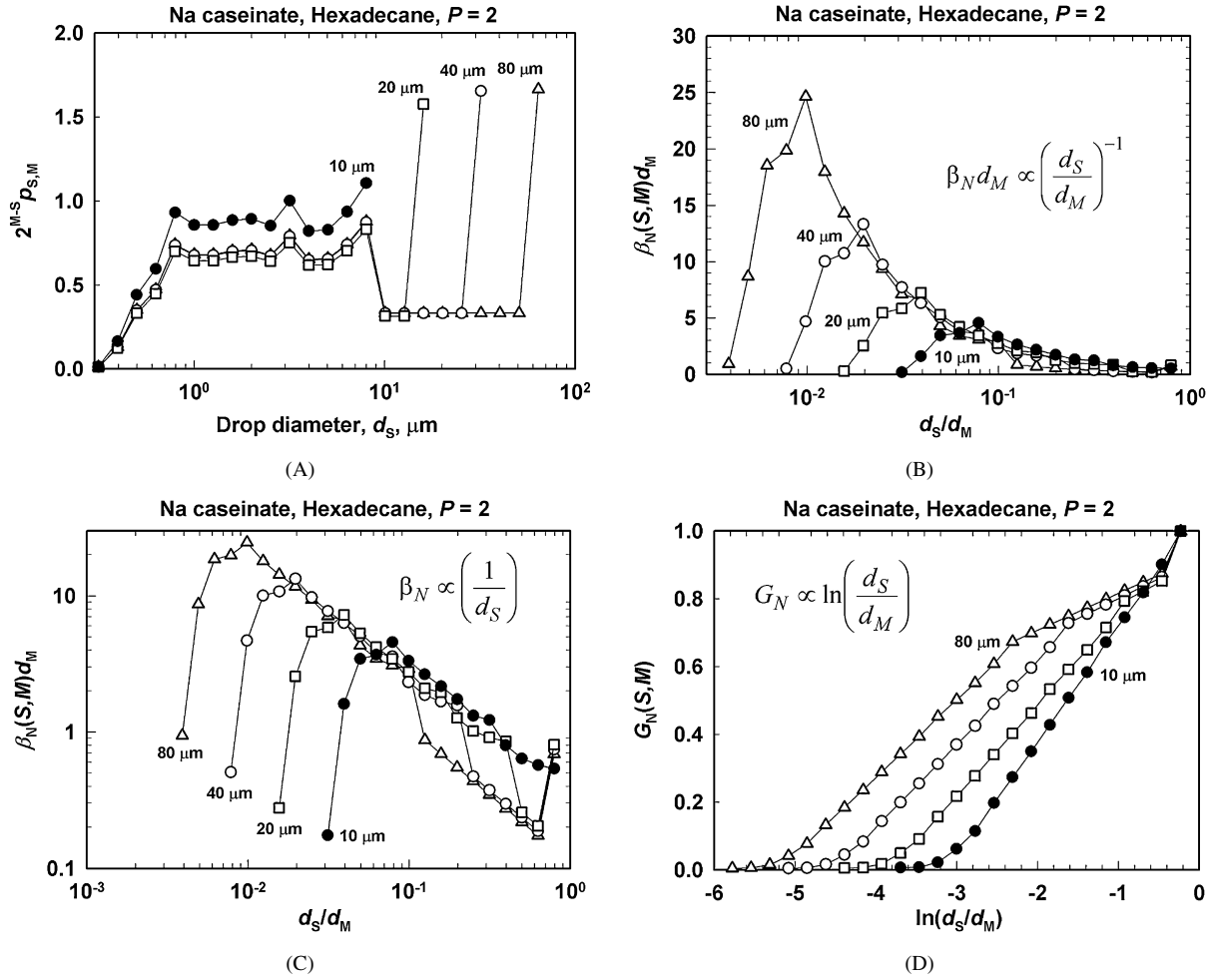

Fig. 8. Experimental results for the daughter drop-size distribution by number for hexadecane emulsion stabilized by Na caseinate (C16_NaC_*P*2) for breaking drops with diameter 10, 20, 40, or 80 μm: (A) $2^{M-S}p_{S,M}$ is the average number of daughter drops with diameter d_S, formed from a breaking drop with diameter d_M; (B) $\beta_N(S,M)$ is distribution function by number, plotted versus the scaled diameter of the daughter drop, d_S/d_M, in linear–log scale; and (C) in log–log scale (D) cumulative distribution by number, $G_N(S,M)$, versus $\ln(d_S/d_M)$. The equations indicate the respective scaling laws, Eqs. (20)–(21).

$$d_M\beta_V(S,M) \propto (d_S/d_M)^2, \tag{20}$$

$$G_N(S,M) \propto \ln(d_S/d_M),$$
$$G_V(S,M) \propto (d_S/d_M)^3. \tag{21}$$

These scaling laws are closely related to the note in Section 4.2 that the data for the hexadecane emulsions could be described rather well by assuming equal probability for formation of daughter drops, down to drop diameter, $d_S \approx 1\ \mu\text{m} \approx 0.1d_D$. Indeed, the assumption that $2^{M-S}p_{S,M}$ is approximately constant, directly leads to $\beta_N(S,M) \propto 2^{M-S}p_{S,M}/\Delta y_S \propto 1/d_S$; the other scaling laws are easily derived from $\beta_N(S,M)$. This observation suggests that Eq. (20) could describe the size distribution of the daughter drops formed in turbulent flow (down to the drop sizes corresponding to the maximum in the histogram peak) for oils with viscosity $\eta_D \approx \eta_C$. The experimental data suggest that the probabilities for formation of the larger daughter drops, $d_S > d_{K+1}$, could follow the same scaling laws (or at least do not deviate much, see Section 4.2), but we could not prove or reject this possibility unambiguously, due to the lack of sufficient experimental accuracy. The probabilities for the very small drops on the left of the peak, $d_S < 0.1d_{K+1}$, rapidly falls down to zero, but again our experimental accuracy was insufficient to determine the precise shape of the functions in this region.

5.3. Dependence of the size distribution of the daughter drops on the oil type

In Figs. 10 and 11 we compare the experimental results for three of the systems, which differ significantly in the viscosity of the oil: hexadecane with $\eta_D = 3.0$ mPa s, and two silicone oils with $\eta_D \approx 50$ and 200 mPa s. For these figures, the diameter of the breaking drop was taken to be the same, $d_M = 50.8$ μm. Similar results for smaller breaking drops, $d_M = d_{K+1} \approx d_D$, are shown for comparison in Fig. 12 for two of these oils (hexadecane and silicone oil with $\eta_D \approx 200$ mPa s).

First, the dependence of the volume probability, $p_{S,M}$, on (d_S/d_M) is shown in Fig. 10A. One sees that for all oils, the value of $p_{S,M}$ passes through a maximum at $d_S/d_M = 0.79$, which corresponds to $v_S/v_M = 0.5$. This maximum is very sharp for hexadecane and less pronounced for the viscous oils

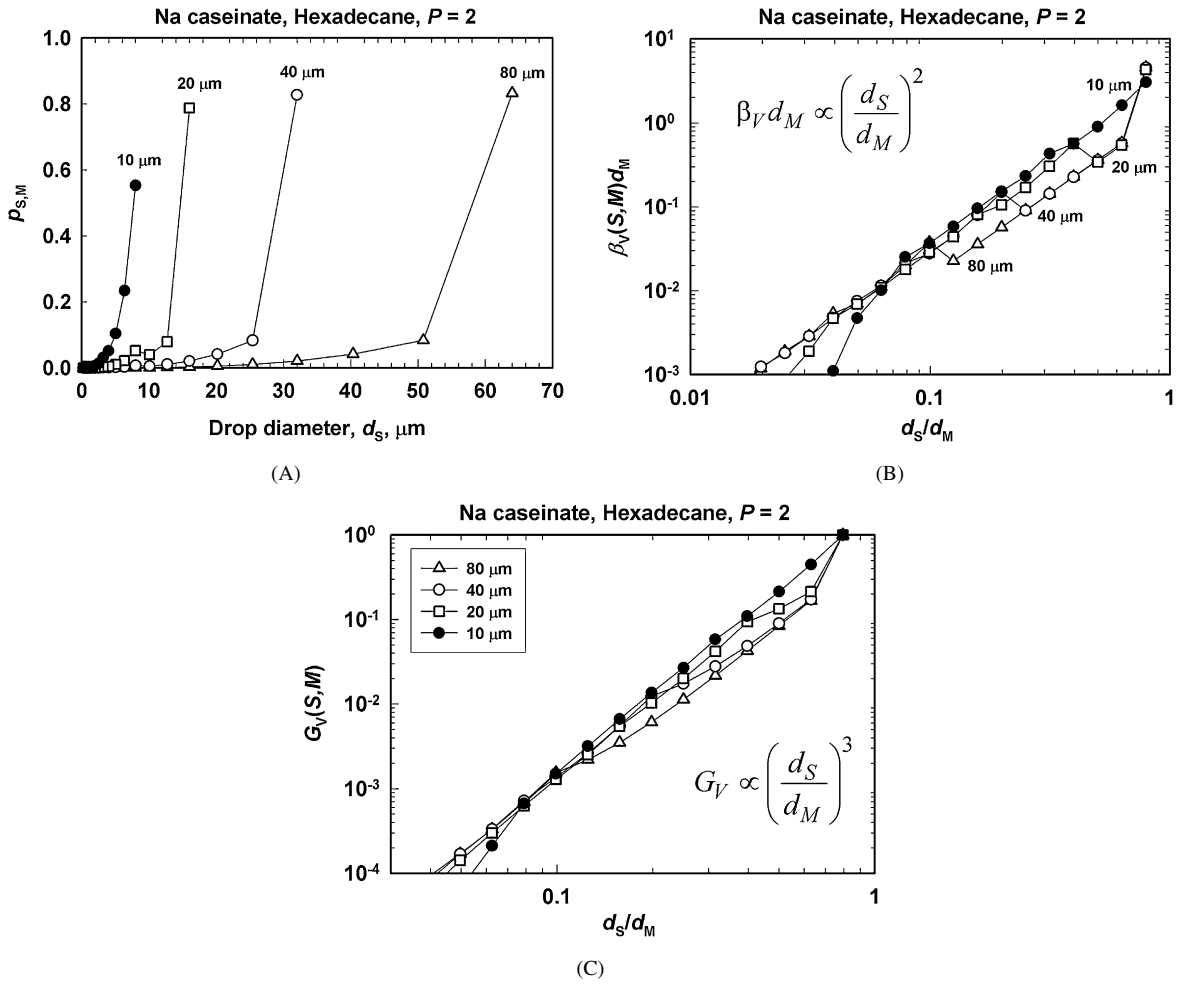

Fig. 9. Experimental results for the size distribution of the daughter drops by volume for hexadecane emulsion stabilized by Na caseinate (C16_NaC_*P*2) for mother drops with diameter 10, 20, 40, or 80 μm: (A) average volume fraction, $p_{S,M}$, of the breaking drop with diameter d_M transformed into daughter drops with diameter d_S; (B) distribution function by volume, $\beta_V(S, M)$, plotted versus the scaled diameter of the daughter drops, d_S/d_M; and (C) cumulative distribution by volume, $G_V(S, M)$, versus d_S/d_M. The equations indicate the respective scaling laws, Eqs. (20)–(21).

(see also Fig. 13 below). Similar is the shape of the respective function $\beta_V(S, M)$ shown in Fig. 10B. The observed maximum of the distribution functions at $v_S/v_M = 0.5$ means that the main fraction of the volume of the mother drop transforms into daughter drops with about twice smaller volume (note, however, the relatively high probability for formation of small daughter drops for the viscous silicone oil). The height of the maximum significantly depends on the oil viscosity—the maximum decreases by several times when the viscosity increases from 3 mPa s (hexadecane) to 200 mPa s (silicone oil), see Fig. 10B. As required by the mass balance, the lower peaks for the more viscous oils correspond to higher probability for formation of smaller drops with diameter $d_S < d_{M-1}$. This effect leads to a very significant increase of the number probability for formation of smaller daughter drops in the case of viscous oils, see Fig. 11A. It is important to note that all distribution functions did not depend strongly on the values of ε and σ, which indicates that the oil viscosity is the key factor, which determines the drop polydispersity in the inertial regime of emulsification (see also the discussion in Section 5.5). The differences between the various oils are reflected also in the cumulative functions by volume, shown in Fig. 10C—for the two silicone oils, $G_V(S, M)$ increases faster in the range of the small daughter drops, whereas the increase for hexadecane is relatively slow in the range of small diameters and rapidly increases as d_S approaches the value corresponding to daughter drops with volume $v_S = v_M/2$.

The distributions by number for these emulsions are compared in Fig. 11 (for clarity only the results for hexadecane and the more viscous silicone oil Sil200 are shown). One can easily discern peaks in the distribution functions for the formed daughter drops, which correspond to the respective peaks in the histograms of the final emulsions, cf. with Figs. 1–3 and Eq. (9). We recall that the different shapes of the curves for $2^{M-S}p_{S,M}$ and $\beta_N(S, M)$, cf. Figs. 11A and 11B, are due to the variable width of the intervals in our discretization scheme. One sees from Fig. 11A that multiple daughter drops (much more than two) are formed in all emulsions and that the number of these drops increases with oil viscosity. The cumulative functions, $G_N(S, M)$, steeply increase in the range of the small diameters, $d_S/d_M < 0.2$ (see Fig. 11C), which shows that the prevailing fraction of the formed drops are with diameter much

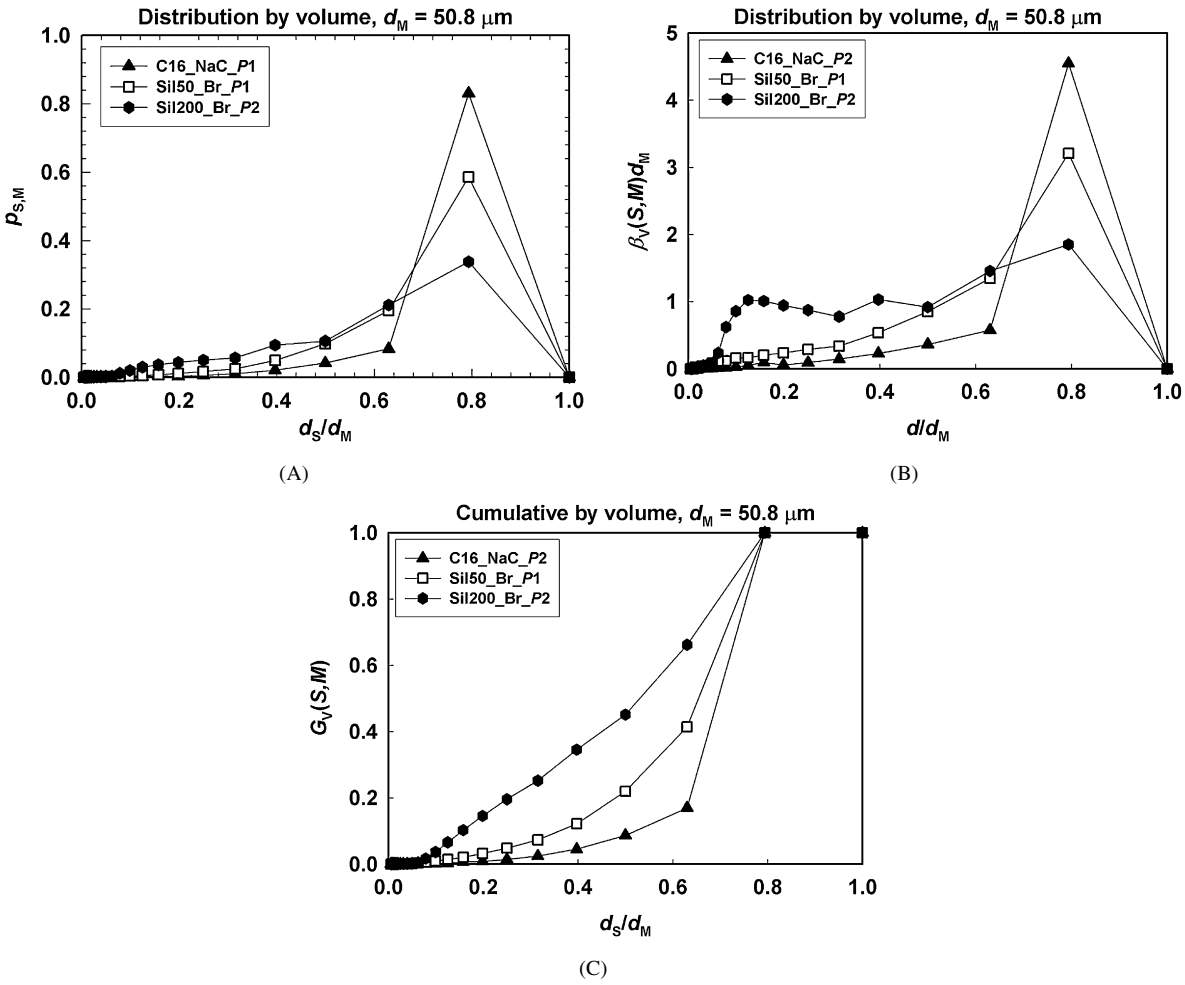

Fig. 10. Experimental results for the size distribution by volume of the daughter drops in emulsions of hexadecane (full triangles, C16_NaC_*P*2), silicone oil 50 (empty squares, Sil50_Br_*P*1), and silicone oil 200 (Sil200_Br_*P*2), for breaking drops with $d_M = 50.8$ μm: (A) $p_{S,M}$; (B) probability distribution by volume, $\beta_V(S, M)$; and (C) cumulative distribution by volume, $G_V(S, M)$, all presented as functions of the scaled diameter of the daughter drops, d_S/d_M.

smaller than that of the breaking drop. Even in the case of the oil with lowest viscosity, hexadecane, more than 70% of the daughter drops (by number) are with diameter $d_S/d_M < 0.2$, corresponding to $v_S/v_M < 0.01$ (and these are most probably satellite drops).

5.4. Comparison of our results with experimental results by other authors

The distribution function by volume for daughter drops formed during emulsification in stirred tanks was determined in Ref. [30] for oil-in-water emulsions of heptane, benzene, and two silicone oils with viscosities 11.3 and 133 mPa s. The comparison of our experimental results for hexadecane and silicone oil with viscosity $\eta_D \approx 200$ (taken for $d_M = d_{K+1}$ in these plots) with those determined in Ref. [30] for benzene, is presented in Fig. 12—one sees that the agreement for the two low-viscosity oils (hexadecane in our experiments and benzene in [30]) is reasonable. Similarly to our results, the experimental results reported by Sathyagal et al. [30] show maximum in the probability function by volume, $\beta_V(d, d_M)$, at $d/d_M \approx 0.8$, whereas the probability function by number, $\beta_N(d, d_M)$, has a maximum at much smaller diameter of the daughter drops, $d/d_M \approx 0.1$. Note that the number of the formed drops from one breaking drop is also similar, ≈11 in our experiments and ≈7 for benzene emulsions in Ref. [30].

For the more viscous oils, the experimental data in Ref. [30] differ qualitatively from our results in the observed trend that the relative contribution of the smaller drops was reported to decrease with the increase of oil viscosity [30], whereas we observed the opposite trend, see Figs. 10–12. This discrepancy is probably caused by the different size ranges of the breaking drops in the two studies (due to the different emulsification procedures used)—the maximum stable drop diameter in our system is 32 μm, whereas it was 250 μm in Ref. [30]. Therefore, we might expect that the contribution of the so-called "satellite drops" with diameter below ca. 2 μm was negligible in Ref. [30], whereas the contribution of these small drops is significant in our systems, see Fig. 12.

Interestingly, our results for the silicone oil with viscosity $\eta_D \approx 200$ mPa s, shown in Fig. 12, evidence that the maximum in the distribution function by volume, $\beta_V(S, M)$, is shifted to the small drop diameters, $d_S/d_M \approx 0.2$, and that the probability for drop formation (by volume) is almost con-

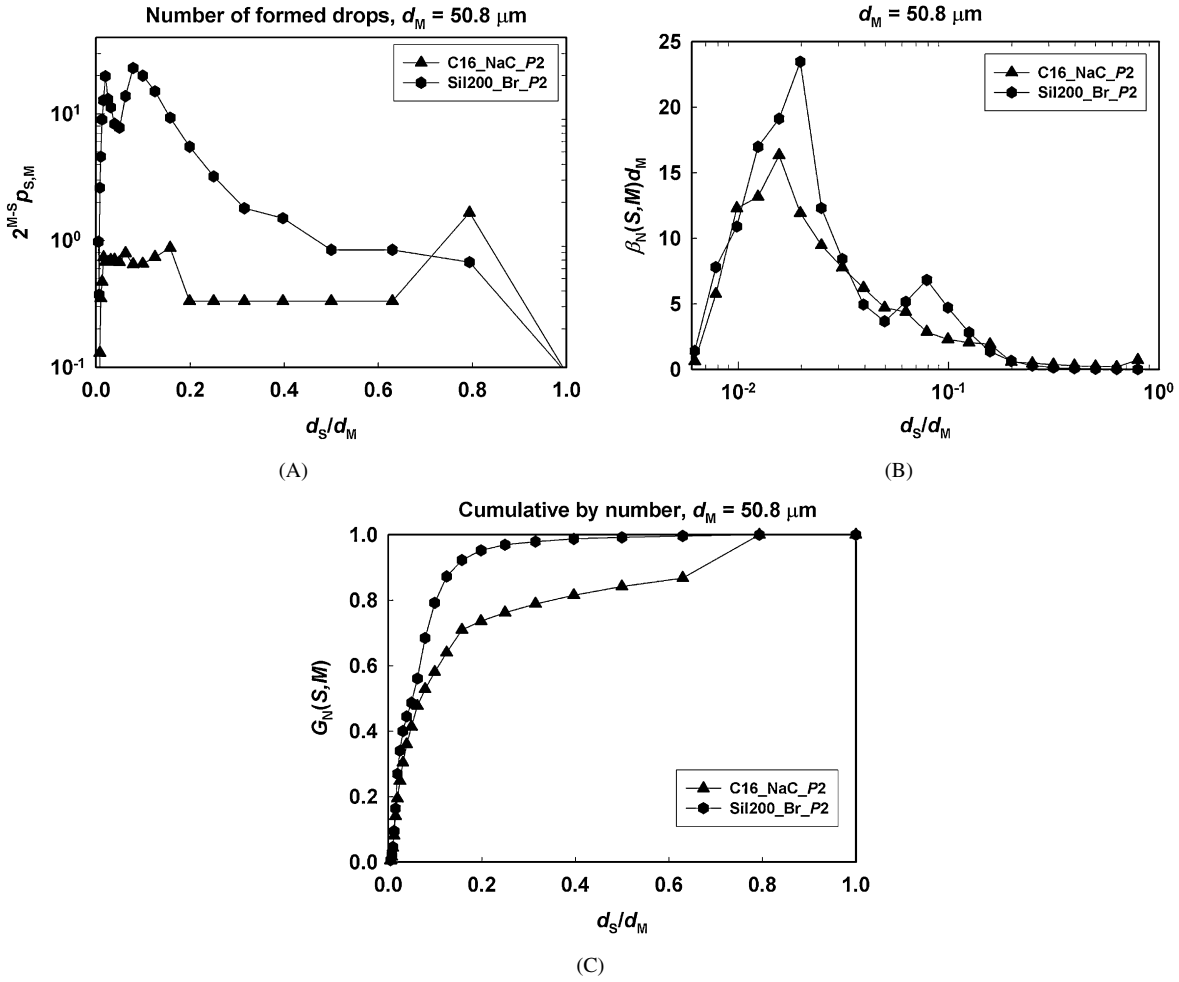

Fig. 11. Experimental results for the size distribution by number of the daughter drops in emulsions of hexadecane (full triangles, C16_NaC_*P*2) and silicone oil 200 (Sil200_Br_*P*2), for breaking drops with $d_M = 50.8$ μm: (A) number of formed drops with diameter d_S, $2^{M-S}p_{S,M}$; (B) discrete distribution function by number, $\beta_N(S, M)$; and (C) cumulative distribution by number, $G_N(S, M)$, all presented as functions of the scaled diameter of the daughter drops, d_S/d_M.

stant in a wide range of scaled diameters of the daughter drops, $0.1 < d_S/d_M < 0.8$ (see also the results in Fig. 10B). This observation suggests that the data for the viscous oils could be described in a certain range of daughter drop diameters by the following scaling laws:

$$d_M\beta_N(S, M) \propto (d_S/d_M)^{-3},$$
$$d_M\beta_V(S, M) \approx \text{const}, \quad 0.1 < d_S/d_M < 0.8, \quad d_M \approx d_D, \tag{22}$$
$$G_N(S, M) \propto (d_S/d_M)^{-2},$$
$$G_V(S, M) \propto (d_S/d_M), \quad 0.1 < d_S/d_M < 0.8, \quad d_M \approx d_D. \tag{23}$$

Similar trends were observed for the other viscous oils, as well (silicone oils with viscosity of 50 and 95 mPa s and Soybean oil) for not-very-large diameters of the breaking drops, $d_M \approx d_D$.

From the values of $p_{S,M}$ we can calculate the average total number of daughter drops, ν, formed after breakage of one mother drop, by the relation:

$$\nu(d_M) = \sum_{S=0}^{M-1} 2^{(M-S)} p_{S,M}. \tag{24}$$

The experimental data for ν, for all studied systems and two different diameters of the breaking drops are presented in Table 1 in Ref. [2]. It is seen that the value of ν increases by more than 5 times with the increase of oil viscosity from 3 to 50 mPa s. The average number of daughter drops increases with the increase of d_M and does not depend strongly on ε and σ. For example, the increase of ε from 0.8×10^5 to 3.4×10^5 J/kg s for hexadecane emulsions leads to an increase of ν from 9 to 11 (cf. cases C16_NaC_p1 and C16_NaC_p2 in Table 1 in Ref. [2]).

The results for hexadecane emulsions (cases C16_Br_p1, C16_NaC_p1, and C16_NaC_p2) are in qualitative agreement with the results reported in Ref. [21], where the average number of formed drops was studied by direct observation of the breakage process of single heptane drops. It was reported in Ref. [21] that the average number of formed drops increased from 2 to 8 while increasing the Weber number from We = 15 to 70. Taking into account that the hexadecane (used by us) is more viscous than heptane ($\eta_D = 0.45$ mPa s), and that the conditions of the experiments in Ref. [21] differed from those in our homogenizer, we can conclude that the agreement between the values of ν determined in both studies are in reasonable agreement.

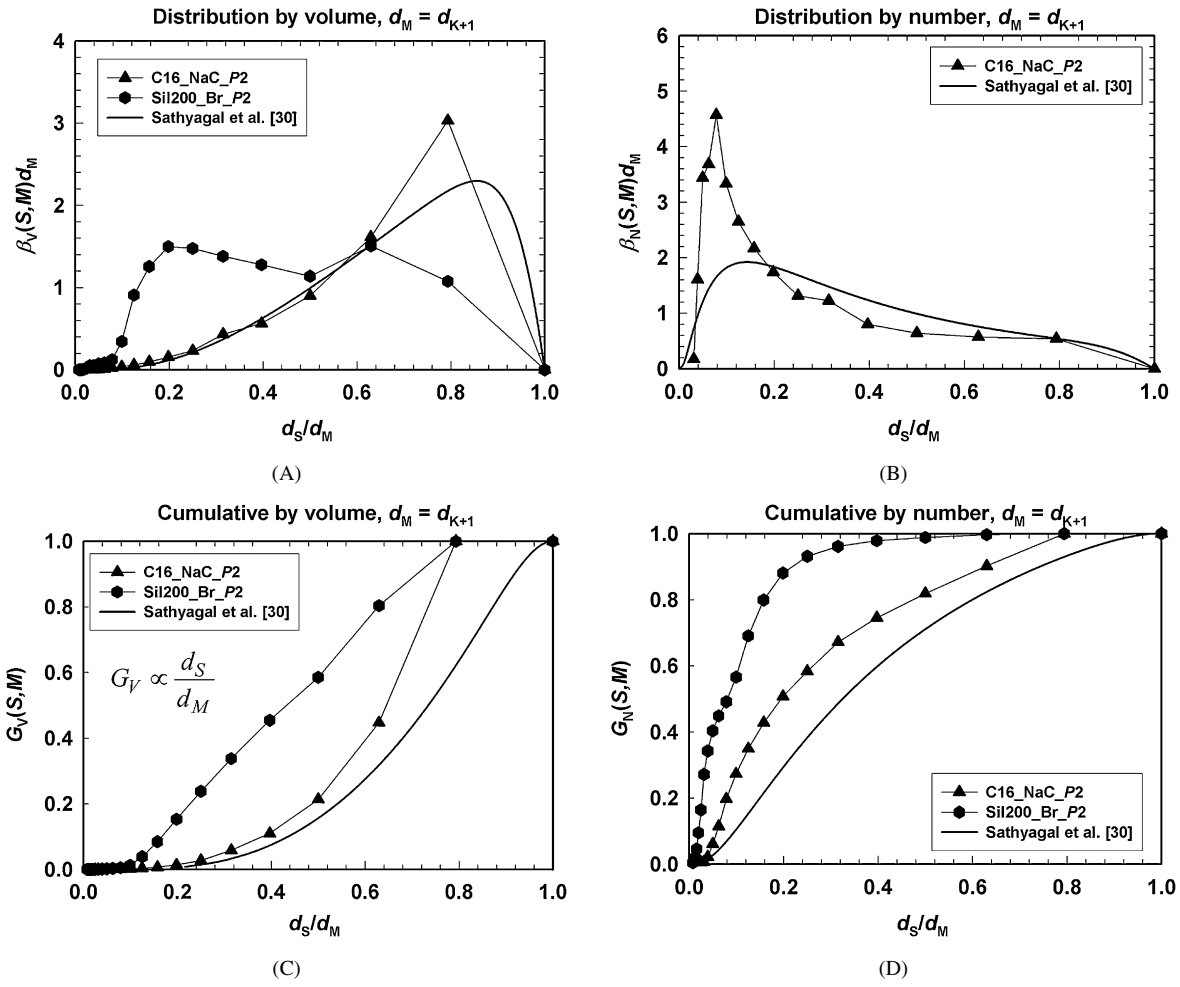

Fig. 12. Comparison of the distributive (A and B) and cumulative (C and D) functions by volume (A and C) and by number (B and D) for emulsions of hexadecane (triangles, C16_NaC_*P*2) and silicone oil 200 (full hexagons, Sil200_Br_*P*2), with the experimentally determined distributions for benzene-in-water emulsions prepared in stirred tank, at 500 rpm, with $d_M = 375$ μm (Ref. [30], continuous curves). In our experiments, $d_M = d_{K+1}$, where $d_{K+1} = 10$ μm for the hexadecane and 32 μm for the silicone oil.

In conclusion, our results for hexadecane are in agreement with the results reported by other authors for not-very-viscous oils. Our results for the viscous oils (soybean oil and silicone oils) show that a larger number of small daughter droplets are formed, see Table 1 in Ref. [2], which might indicate possible differences in the mechanism of drop breakage for oils with low and high viscosities—see the discussion at the end of Section 5.5.

5.5. Comparison of the experimental results with model theoretical functions, proposed in the literature

As mentioned in the Introduction, three main types of models for the daughter drop-size distribution are discussed in literature—statistical, phenomenological (based on the change in the surface energy of the breaking drops), and hybrid [14]. Several of the statistical models [15,31,32] predict highest probability for formation of drops with equal volume $v = v_M/2$, as observed in many of our experiments. Below, we compare our results with one of the basic models of this type, proposed by Coulaloglou and Tavlarides [15], which is denoted below as the "CT model." Our numerical checks showed that the comparison with the other model distributions of this type [31,32] leads to similar conclusions.

In the CT model [15], two daughter drops are assumed to form in each drop breakage event and these drops could be of different size. The probability for formation of these drops is assumed to be normally distributed around the drops with volume, $v = v_M/2$. The width of the normal distribution is chosen in such a way that 99.6% of the formed drops fall in the volume range between 0 and v_M, which results in the following distribution function by number [15]:

$$\beta_N^{\mathrm{CT}}(v, v_M) = \frac{2.4}{v_M} \exp\left[-4.5\left(2(v/v_M) - 1\right)^2\right], \tag{25}$$

where the volume of the daughter drop, v, is considered as continuous variable. This function presents the number probability for formation of drops within the interval between v and $v + \delta v$. To determine the probability for formation of daughter drops within the interval of diameters between d and $d + \delta d$, we should change the variable in Eq. (25) and take into account that $\delta v = (\pi/2)d^2\delta d$. The corresponding probability function

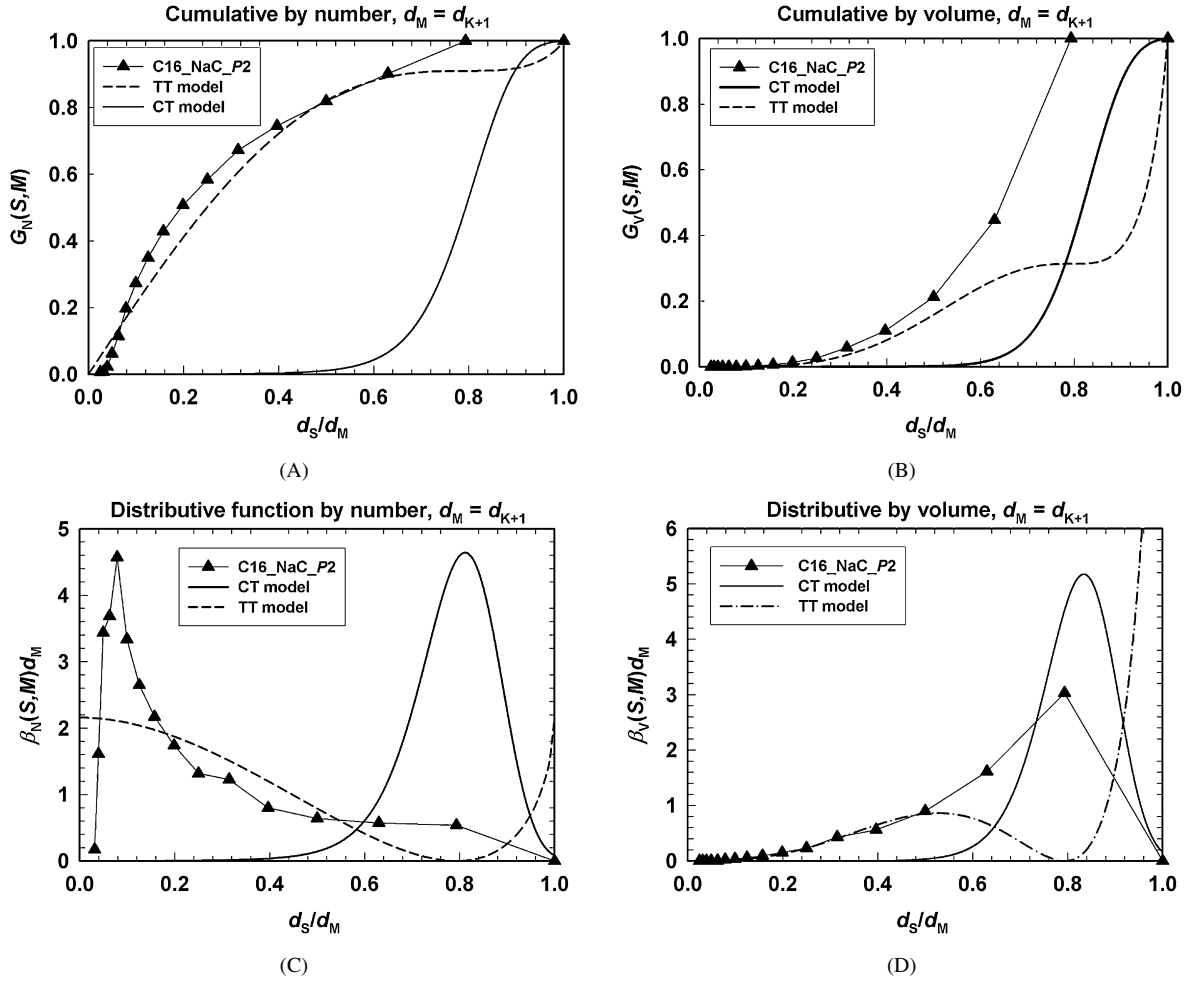

Fig. 13. Cumulative functions by (A) number and (B) volume and distributive functions by (C) number and (D) volume for hexadecane emulsions (triangles, C16_NaC_*P*2) along with the theoretical curves calculated by using the CT-model from Ref. [15] (the dashed curves) and the TT-model from Ref. [19] (the solid curves).

reads

$$\beta_N^{\mathrm{CT}}(d,d_M) = \frac{7.2}{d_M}\left(\frac{d}{d_M}\right)^2 \exp\left[-4.5\left(2(d/d_M)^3-1\right)^2\right]. \quad (26)$$

The respective cumulative function is obtained by integrating Eq. (26):

$$G_N^{\mathrm{CT}}(d,d_M) = \int_0^d \beta_N^{\mathrm{CT}}(d,d_M)\delta d \approx 0.5\left[1+\mathrm{erf}\left(2.12\left(2\frac{d^3}{d_M^3}-1\right)\right)\right]. \quad (27)$$

The distributive and cumulative functions by volume are also of interest. Starting from Eq. (25), one derives the following distributive function by volume for the CT model:

$$\beta_V^{\mathrm{CT}}(d,d_M) = \frac{d^3\beta_N^{\mathrm{CT}}(d,d_M)}{\int_0^{d_M} d^3\beta_N^{\mathrm{CT}}(d,d_M)\delta d} \approx \frac{14.4}{d_M}\left(\frac{d}{d_M}\right)^5 \exp\left[-4.5\left(2(d/d_M)^3-1\right)^2\right]. \quad (28)$$

This function expresses the volume fraction of the formed daughter drops falling in the interval between d and $d+\delta d$. The respective cumulative function by volume is

$$G_V^{\mathrm{CT}}(d,d_M) \approx 0.5\left\{1-\mathrm{erf}\left[2.12\left(1-2\frac{d^3}{d_M^3}\right)\right] - 0.00295\exp\left[18\left(\frac{d^3}{d_M^3}\right)\left(1-\frac{d^3}{d_M^3}\right)\right]\right\}. \quad (29)$$

Due to the self-similarity assumption implemented in the CT model, all these functions depend on the ratio (d/d_M) only.

Before comparing the predictions of the CT model with our results, let us introduce one of the main phenomenological models, which are based on consideration of the surface energy of the breaking drop. The phenomenological models usually predict lowest probability for formation of daughter drops with volume $v = v_M/2$, see Refs. [17–19,29]. As representative of this class of models we consider the model by Tsouris and Tavlarides [19] (denoted as TT model), which predicts zero probability for formation of drops with equal volume. The dis-

tributive function by number in this model is defined as

$$\beta_N^{\mathrm{TT}}(d,d_M)=\frac{E_{\mathrm{MIN}}+E_{\mathrm{MAX}}-E(d)}{\int_0^{d_M}[E_{\mathrm{MIN}}+E_{\mathrm{MAX}}-E(d)]\delta d}, \tag{30}$$

where E_{MIN} is the surface energy needed to create the smallest and the largest daughter drops, E_{MAX} is the energy needed to create two equal drops and $E(d)$ is the energy needed to create a pair of drops, one of which has diameter d. Following the assumptions from Ref. [19], $E_{\mathrm{MIN}}\approx 0$, $E_{\mathrm{MAX}}=\pi\sigma(2^{1/3}-1)d_M^2$, and $E(d)=\pi\sigma[d^2+(1-d^3)^{2/3}-d_M^2]$, we obtain

$$\beta_N^{\mathrm{TT}}(d,d_M)=\Big\{10.5-8.34\Big[(d/d_M)^2+\big(1-(d/d_M)^3\big)^{2/3}\Big]\Big\}/d_M. \tag{31}$$

The respective cumulative function by number can be found through the expression:

$$G_N^{\mathrm{TT}}(d,d_M)=\left[\int_0^d \beta_N^{\mathrm{TT}}(d,d_M)\delta d\right]\Big/\left[\int_0^{d_M}\beta_N^{\mathrm{TT}}(d,d_M)\delta d\right]. \tag{32}$$

The distributive function by volume in the TT model is expressed as

$$\beta_V^{\mathrm{TT}}(d,d_M)=d^3\Big[90.1-71.5\Big((d/d_M)^2+\big(1-(d/d_M)^3\big)^{2/3}\Big)\Big]/d_M^4 \tag{33}$$

and the respective cumulative function can be found by integration (see Eq. (32)).

In the following part of this section, we compare our results from the emulsification experiments with the predictions of the two basic theoretical models described above. The results obtained with hexadecane are compared in Fig. 13 with the predictions of the CT and TT models. One sees from Fig. 13A that the TT model describes reasonably well the main trend in the experimentally determined cumulative function, $G_N(S,M)$. In contrast, the CT model strongly underestimates the number of formed drops in the entire range of sizes of daughter drops. Concerning the cumulative function by volume, Fig. 13B, we see that the CT model deviates significantly from the experimental results, whereas the TT model describes reasonably well the results for the small daughter drops, $d_S/d_M<0.5$. The comparison of the experimentally determined distributive function by volume, β_V, with the predictions of the CT and TT models (Fig. 13D) shows a reasonably good agreement only for the TT model in the range of small drop diameters. In the region of the larger diameters of the daughter drops, $d_S/d_M\approx 0.8$ (corresponding to $v_S/v_M=0.5$) the TT model predicts zero probability, whereas the experimental data show maximum probability of drop formation. The agreement with the CT model is rather poor in the entire range of drop sizes, except for the region $d_S/d_M\approx 0.8$, where the CT model predicts maximum probability in agreement with the experimental results. The distributions by number are not described well by any of these models, see Fig. 13C. Even the TT model, which describes reasonably well the experimental data by volume for small drop diameters, deviates significantly from the experimentally determined distribution function by number. Note that the experimental probability exhibits a maximum at a certain diameter of the daughter drops, $d_S/d_M\approx 0.1$, whereas no such feature is suggested by any of these models. Also, the CT and TT models cannot describe the experimental results for any of the more viscous oils, $\eta_D\gg 1$ mPa s, because the models strongly underestimate the large number of small droplets with $d_S/d_M<0.5$, which are formed in these emulsions, see Figs. 10–12. One can conclude from this comparison that these basic models need a significant modification to describe the experimental results for the emulsions studied.

Let us discuss briefly the main features of the experimental results, which should be captured by the model distribution functions. Both sets of experimental data, ours and those in Ref. [30], show that the distribution function *by volume* for oils of low viscosity (hexadecane, benzene) has a maximum at $d_S/d_M\approx 0.8$. Also, a significant fraction of the distribution function is described by the scaling laws, see Eqs. (20)–(21), which should be implemented in the model function for the size range $0.1d_D<d_S<0.8d_D$. Note that for the viscous oils we observed different scaling laws, Eqs. (22)–(23), which shows that the model function should depend significantly on the oil viscosity.

As seen from Figs. 11 and 13C, the model distribution functions *by number* should pass through a maximum at $\approx 0.1d_D$. The respective scaling laws should be also implemented in the model function within the range $0.1d_D<d_S<0.8d_D$. Note that our data do not require symmetric functions with respect to $v_S/v_M=0.5$ (corresponding to $d_S/d_M\approx 0.8$), which is the case with most model functions proposed in the literature. The main reason is that our results evidence that the breakage of one drop leads to formation of many daughter drops, whereas the symmetry implemented in most of the model functions follows from the (unjustified) assumption for a binary breakage of the mother drop.

At the end, let us note that our results indicate that the daughter drops are formed (especially in the case of viscous oils) mainly through the mechanism of capillary instability of long oil threads, which are formed upon deformation of the viscous oil drops in the turbulent flow—see Fig. 14 for illustration. Indeed, if the multiple daughter drops were formed as a result of "biting" of small portions of the mother drop by small turbulent eddies, one should expect that larger number of drops would be formed in the case of less viscous oils, for which this "biting" process is expected to be more efficient (due to the faster deformation time and the lower energy requirements). The experimental fact that much larger number of daughter drops is observed with the more viscous oils is a clear indication that these drops appear as a result of another process, with the most probable option being the capillary driven subdivision of long oily threads, which are formed upon the deformation of viscous drops (Fig. 14). Therefore, one possible approach to construct model functions for the daughter drop-size distribution could be to try a combination of the models for drop breakage in turbulent flow (to describe the initial stage of drop deformation

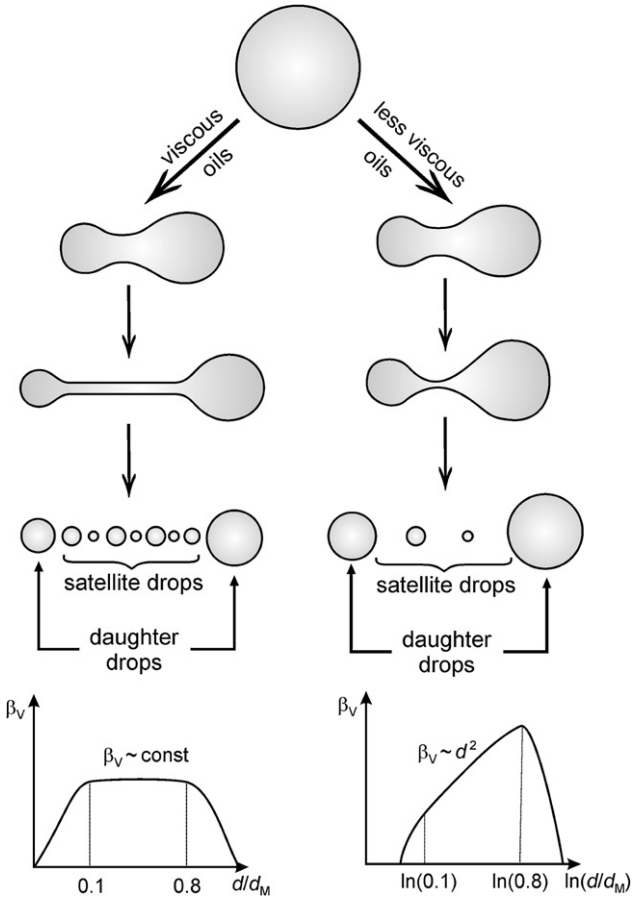

Fig. 14. Schematic presentation of the process of drop breakage of mother drops of less-viscous and more viscous oils with $d_M \approx d_D$ (see the results in Figs. 8–10 and 12).

and thread formation) with the models for thread breakage by capillary instability (similar to those developed for drop breakage in shear flows). The construction of such "universal" model function, describing the size distribution of daughter drops in the case of oils with different viscosities, is a very interesting, but challenging problem, so that it falls beyond the scope of the present study.

6. Conclusions

Systematic set of experiments is performed to monitor the evolution of the drop-size distribution, as a function of the emulsification time, in turbulent flow. The effects of the viscosity of the oil phase, η_D, interfacial tension, σ, and rate of energy dissipation, ε, are studied.

From the experimental results we were able to determine the drop-size distribution of the daughter drops formed upon breakage of a larger drop. For data analysis we proposed a new "combined model," see Eqs. (9) and (11)–(14), which is essentially based on the assumption that the probability for formation of daughter drops with diameter smaller than the maximum diameter of the stable drops, $d_S < d_D$, is proportional to the drop concentrations in the final emulsions (these concentrations are easily determined experimentally, Figs. 1–3). The proposed model contains only one adjustable parameter, related to the daughter drop-size distribution (denoted as b_2 in Eq. (11)), which is determined by the best fit to the experimental data, along with the kinetic constants of drop breakage, k_{BR}.

We have found that the daughter drop-size distribution depends significantly on the viscosity of the dispersed phase. For oils with low viscosity, the probability for daughter drop formation (by volume) has maximum for drops with volume, which is twice smaller than the volume of the breaking drop, Figs. 10 and 13. In contrast, the probability for formation of much smaller daughter drops is rather high for the viscous oils, Figs. 10–12. Different scaling laws are found to describe the experimental data for the oils of low and high viscosity, Eqs. (22)–(23).

The experimentally determined size distributions of the daughter drops are compared with model functions proposed in the literature and with experimental results by other authors. Our results for the oil of low viscosity (hexadecane) are in good agreement with the corresponding experimental results by Sathyagal et al. [30], Fig. 12. The results for the more viscous oils differ substantially, which is explained by the significant contribution of the small daughter drops in our experiments. The comparison with some basic model functions did not show good agreement and the possible reasons for this discrepancy are discussed, Figs. 13–14. The most important reason is that our results show clearly that multiple daughter drops are formed upon breakage of a single mother drop, whereas the basic theoretical models usually assume binary breakage. The experiments show that the total number of daughter drops strongly increases with the viscosity of the oil, see Table 1 in Ref. [2], and the possible mechanism leading to this result is illustrated in Fig. 14 and discussed in Section 5.5.

The proposed numerical procedure allowed us to describe with very good accuracy the evolution of all main characteristics of the drop-size distribution in the emulsions during emulsification, such as the various mean diameters, and the distributive and cumulative functions by number and by volume (see Figs. 5–7).

Acknowledgments

The authors are grateful to Prof. I.B. Ivanov for the useful discussions and for the critical reading of the manuscript. The useful discussion with Prof. M. Kostoglou (Aristotle University, Thessaloniki, Greece) is gratefully acknowledged. The valuable experimental help by D. Sidzhakova and the help in drop-size determination by M. Paraskova and E. Kostova (all from the Sofia University) are deeply appreciated. This study was supported by BASF Aktiengesellschaft, Ludwigshafen, Germany.

Appendix A. Notation

To save space, only the notation that did not appear in the first and second parts of this series, Refs. [1,2], is listed below.

Capital Latin letters

E energy

E_{MAX} energy needed for creation of two drops of equal diameters

E_{MIN} surface energy for creation of the smallest and the largest daughter drops in the literature models assuming binary breakage

$E(d)$ energy needed for creation of a pair of drops, one of which has diameter d

G cumulative distribution function for daughter drops

$G_N(S, M)$ discrete cumulative function by number

$G_V(S, M)$ discrete cumulative function by volume

$G_N(d, d_M)$ continuous cumulative function by number

$G_V(d, d_M)$ continuous cumulative function by volume

$G_N^{CT}(d, d_M)$ cumulative function by number in the "CT model"

$G_V^{CT}(d, d_M)$ cumulative function by volume in the "CT model"

$G_N^{TT}(d, d_M)$ cumulative function by number in the "TT model"

$G_V^{TT}(d, d_M)$ cumulative function by volume in the "TT model"

Small Latin letters

b constants

b_1 numerical constant denoting the number probability $(2^{M-S}p_{S,M})$ for formation of drops in the interval from K to $(M-1)$, Eq. (8)

b_2 adjustable parameter denoting the ratio $p_{M-1,M}/p_{M-2,M}$ for arbitrary M

b_3 numerical constant denoting the number probability $(2^{M-S}p_{S,M})$ for formation of drops in the interval from K to $(M-2)$, Eq. (12)

b_M constant of proportionality in the expression for the number probability for formation of drops with $d < d_K$, Eqs. (9), (10)

d drop diameter

d_{K+1} diameter of the smallest drops that can break

d_{M-1} diameter of the largest daughter drops, formed after breakage of a mother drop with diameter d_M

d_{43} mass-averaged mean diameter

d_{10} experimentally measured mean diameter by number

v volume of a daughter drop, considered as continuous variable in the "CT model," Eq. (25)

Small Greek letters

β distribution function

$\beta_N(S, M)$ discrete distribution function by number

$\beta_V(S, M)$ discrete distribution function by volume

$\beta_N(d, d_M)$ continuous distribution function by number

$\beta_V(d, d_M)$ continuous distribution function by volume

$\beta_N^{CT}(d, d_M)$ distribution function by number in the "CT model" (expressed through the diameters of the daughter and mother drops, d and d_M); presents the number probability for formation of drops within the interval between d and $d + \delta d$

$\beta_N^{CT}(v, v_M)$ distribution function by number in the "CT model" (expressed through the volumes of the daughter and mother drops, v and v_M); presents the number probability for formation of drops within the interval between v and $v + \delta v$

$\beta_V^{CT}(d, d_M)$ distribution function by volume in the "CT model"

$\beta_N^{TT}(d, d_M)$ distribution function by number in the "TT model"

$\beta_V^{TT}(d, d_M)$ distribution function by volume in the "TT model"

ν average total number of daughter drops, formed after breakage of a mother drop

Abbreviations

CT model theoretical model for the daughter drop-size distribution, proposed by Coulaloglou and Tavlarides [15]

TT model theoretical model for the daughter drop-size distribution, proposed by Tsouris and Tavlarides [19]

Supplementary material

The online version of this article contains additional supplementary material.

Please visit DOI: 10.1016/j.jcis.2007.01.097.

References

[1] N. Vankova, S. Tcholakova, N.D. Denkov, I.B. Ivanov, V. Vulchev, T. Danner, Emulsification in turbulent flow: 1. Mean and maximum drop diameters in inertial and viscous regimes. First paper of this series.
[2] N. Vankova, S. Tcholakova, N.D. Denkov, V. Vulchev, T. Danner, Emulsification in turbulent flow: 2. Breakage rate constants. Second paper of this series.
[3] A.N. Kolmogorov, Compt. Rend. Acad. Sci. URSS 66 (1949) 825.
[4] J.O. Hinze, AIChE J. 1 (1955) 289.
[5] J.T. Davies, Chem. Eng. Sci. 40 (1985) 839.
[6] R.V. Calabrese, T.P.K. Chang, P.T. Dang, AIChE J. 32 (1986) 657.
[7] C.Y. Wang, R.V. Calabrese, AIChE J. 32 (1986) 667.
[8] R.V. Calabrese, C.Y. Wang, N.P. Bryner, AIChE J. 32 (1986) 677.
[9] P.D. Berkman, R.V. Calabrese, AIChE J. 34 (1988) 602.
[10] J.S. Lagisetty, P.K. Das, R. Kumar, K.S. Gandhi, Chem. Eng. Sci. 41 (1986) 65.
[11] S. Tcholakova, N.D. Denkov, D. Sidzhakova, I.B. Ivanov, B. Campbell, Langmuir 19 (2003) 5640.
[12] S. Tcholakova, N.D. Denkov, T. Danner, Langmuir 20 (2004) 7444.
[13] H. Steiner, R. Teppner, G. Brenn, N. Vankova, S. Tcholakova, N.D. Denkov, Chem. Eng. Sci. 61 (2006) 5841.
[14] J.C. Lasheras, C. Eastwood, C. Martinez-Bazan, J.L. Montanes, Int. J. Multiphase Flow 28 (2002) 247.
[15] C.A. Coulaloglou, L.L. Tavlarides, Chem. Eng. Sci. 32 (1977) 1289.
[16] M. Konno, Y. Matsunaga, K. Arai, S. Saito, J. Chem. Eng. Jpn. 16 (1980) 67.
[17] D.K.R. Nambiar, R. Kumar, T.R. Das, K.S. Gandhi, Chem. Eng. Sci. 47 (1992) 2989.
[18] D.K.R. Nambiar, R. Kumar, T.R. Das, K.S. Gandhi, Chem. Eng. Sci. 49 (1994) 2194.
[19] C. Tsouris, L.L. Tavlarides, AIChE J. 40 (1994) 395.
[20] M. Konno, M. Aoki, S. Saito, J. Chem. Eng. Jpn. 16 (1983) 312.
[21] S. Galinat, O. Masbernat, P. Guiraud, C. Dalmazzone, C. Noik, Chem. Eng. Sci. 60 (2005) 6511.
[22] H. Stone, Annu. Rev. Fluid Mech. 26 (1994) 65.
[23] J.M.H. Janssen, H.E.H. Meijer, J. Rheol. 37 (1993) 597.
[24] J.M.H. Janssen, H.E.H. Meijer, Polym. Eng. Sci. 35 (1995) 1767.
[25] M. Kostoglou, A.J. Karabelas, Chem. Eng. Sci. 60 (2005) 6584.
[26] K.J. Valentas, O. Bilous, N.R. Amundson, Ind. Eng. Chem. Fundam. 5 (1966) 271.
[27] M.J. Prince, H.W. Blanch, AIChE J. 36 (1990) 1485.
[28] C. Orr, in: Encyclopedia of Emulsion Technology, Dekker, New York, 1983, Chapter 6.

[29] H. Luo, F. Svendsen, AIChE J. 42 (1996) 1225.
[30] A.N. Sathyagal, D. Ramkrishna, G. Narsimhan, Chem. Eng. Sci. 9 (1996) 1377.
[31] A.M. Hsia, L.L. Tavlarides, Chem. Eng. J. 26 (1983) 189.
[32] C.H. Lee, L.E. Erickson, L.A. Glasgow, Chem. Eng. Commun. 61 (1987) 181.